RSC
Applied Interfaces

ROYAL SOCIETY OF CHEMISTRY

REVIEW

View Article Online
View Journal

Cite this: DOI: 10.1039/d6lf00017g

2D nanomaterials: pioneering platforms for cancer theranostics

Akanshya Mishra and Jasaswini Tripathy *

Received 23rd January 2026,
Accepted 6th May 2026

DOI: 10.1039/d6lf00017g

rsc.li/RSCApplInter

Two-dimensional (2D) materials, owing to their distinctive physicochemical properties, are increasingly prominent in biomedicine. These materials have been widely utilized in photothermal therapy, imaging, drug delivery, and many combined therapies. Owing to their unique characteristics, 2D nanoparticles deliver therapeutic effects through diverse mechanisms, demonstrating significant potential for clinical applications. This review highlights the development and biomedical applications of 2D nanomaterials. It begins by introducing the structures, biological functionalization, and properties of representative 2D nanomaterials with varying configurations, along with their associated biomedical uses. Next, it explores the capabilities of 2D nanomedicines in therapeutics, imaging, and drug delivery. Finally, challenges and prospects for the clinical translation of 2D nanomedicines are discussed.

1. Introduction

Cancer is considered a serious, life-threatening disease that is spreading rapidly. It remains the second leading cause of death despite advances in science, technology, and medicine.[1] The complex and varied origins of cancer make it difficult to treat. Many cancer cells are resistant to multiple drugs, which leads to the failure of many traditional treatments when used alone. Cancer cells can easily develop resistance to a treatment if they have been used once.[2] This inherent as well as acquired capability of resistance is central to perhaps one of the most formidable problems in oncology today. The major factor in chemotherapy ineffectiveness is multidrug resistance (MDR), resulting in reduced efficacy of chemotherapy as well as increased medical problems. This is largely mediated by various surface-related mechanisms such as P-glycoprotein and MDR protein 1, which act as efflux pumps that actively pump chemotherapeutic drugs out of cancer cells to prevent them from entering these cells. Besides these biological obstacles to chemotherapeutic

School of Applied Sciences (Chemistry), KIIT Deemed to be University, Bhubaneswar-751024, India. E-mail: jtripathyfch@kiit.ac.in

Akanshya Mishra

Akanshya Mishra received her Integrated M.Sc. degree in Applied Chemistry from Odisha University of Technology and Research, Bhubaneswar, India, in 2022. Currently, she is pursuing her Ph.D. in the School of Applied Sciences at the Kalinga Institute of Industrial Technology, Bhubaneswar, India, under the supervision of Dr. Jasaswini Tripathy. Her current research focuses on the synthesis of two-dimensional (2D) nanomaterial-based hybrid systems, their characterization, and diverse applications.

Jasaswini Tripathy

Jasaswini Tripathy is currently working as an Associate Professor in the Department of Chemistry at the School of Applied Sciences, Kalinga Institute of Industrial Technology (KIIT), Bhubaneswar, India. She obtained her Ph.D. degree from the University of Allahabad, Prayagraj, India, in 2008. Following her doctoral studies, she worked as a DST-funded research scientist at the National Institute of Pharmaceutical Education and Research (NIPER), Mohali, India. She then pursued postdoctoral research at the Indian Institute of Science (IISc), Bengaluru, India, from 2009 to 2013. Her research primarily focuses on the synthesis, characterization, and diverse applications of nanomaterials.

efficacy, various therapeutic approaches are further hindered by the low bioavailability, poor aqueous solubility, and high blood clearance of first-line chemotherapeutic drugs, often leading to increased doses that result in systemic toxicity.[3–6]

Two-dimensional (2D) nanomaterials with a flat-sheet nanostructure exhibit notable physicochemical properties, including a large surface area, unique optical properties, and distinctive surface chemistry. These features make them highly promising for various biomedical applications.[7–19] Moreover, various nanoparticles, such as gold, inorganic quantum dots, and iron oxide nanoparticles, can be attached to the surfaces of 2D nanomaterials. These modifications enhance their functionality, conferring properties such as magnetic effects, radioactivity, and electrochemical activity.[12,20–22]

The emergence of graphene and its potential applications have prompted researchers to investigate other types of 2D nanomaterials, like layered double hydroxides (LDHs),[23–25] black phosphorus (BP) nanosheets,[25–29] transition metal carbides, nitrides, and carbonitrides (MXenes),[30–32] 2D metal–organic frameworks (MOFs),[33–36] transition metal dichalcogenides (TMDs),[37–42] hexagonal boron nitride (hBN) nanosheets,[43] 2D boron (B) nanosheets[44] antimonene (AM) nanosheets,[45,46] and palladium (Pd) nanosheets.[47] Various methodologies have been developed for synthesizing these 2D nanomaterials, including liquid-phase exfoliation,[48,49] hydrothermal, solvothermal, and mechanical exfoliation,[42,50] and chemical vapor deposition (CVD).[51–53] These methods generally fall into two main categories: top-down and bottom-up approaches. These 2D nanomaterials have emerged as a significant point for scientists and engineers across multiple disciplines, including catalysis, solar energy, electronics, and biomedicine.[54]

Due to their atomically thin structure and distinctive physicochemical properties, 2D nanomaterials have attracted considerable attention as versatile candidates in biomedical science. Their sheet-like morphology offers an exceptionally high surface-to-volume ratio, which facilitates efficient drug encapsulation, strong biomolecular interactions, and enhanced cellular uptake.[55] Moreover, the abundance of reactive surface sites allows straightforward modification with polymers, ligands, or therapeutic cargos, enabling highly targeted and controlled delivery. The surface area of 2D nanomaterials is the highest among all material types due to their ultrathin structure. Their extensive surface area enables efficient modification with various functional groups, such as bio-macromolecules, fluorescent probes, and chemotherapeutic agents, via covalent or non-covalent interactions.[56] Their ability to tune their optical, electronic, and mechanical properties further expands their use in biosensing, diagnostic imaging, photothermal therapy, and regenerative medicine. Notably, their strong near-infrared (NIR) absorption and efficient photothermal conversion make them excellent agents for minimally invasive cancer treatments, while their favorable biocompatibility and capacity to modulate the extracellular environment highlight their promise in tissue repair and engineering. Altogether, these attributes establish 2D nanomaterials as a dynamic platform for advancing next-generation biomedical technologies.[57]

Additionally, many 2D nanomaterials exhibit strong NIR absorption, making them promising agents for photothermal therapy (PTT) in cancer treatment.[28] Considering these exceptional properties, 2D nanomaterials have become promising nanoplatforms for a range of theranostic applications in cancer therapy.[58,59] This review summarizes recent advancements reported by researchers on the design of diverse 2D nanomaterials and their applications in cancer theranostics.

2. Synthesis strategies of 2D nanoparticles

2.1. Top-down method

Top-down methods primarily use liquid-phase exfoliation (LPE) and mechanical techniques. These methods are advantageous for weakening the van der Waals interactions that hold layers together in bulk materials. A top-down synthetic process is easy to reproduce and cost-effective. Micromechanical cleavage and ball milling are part of the mechanical exfoliation methods. In micromechanical cleavage, adhesive tape is used to peel off thin 2D flakes, called crystals, from bulk materials.[60–62]

Covalent bonds within the layers of 2D materials remain intact, while the interlayer spacing is expanded.[63] These 2D sheets are relatively large, providing high-quality, impurity-free surfaces and flexibility for a wide range of applications. In ball-milling exfoliation, shear and compression forces work together to separate bulk layered materials into single or few-layer sheets.[57] The resulting materials typically have dimensions around 200 nm and are suitable for different 2D materials. This technique has been used to produce nanomaterials such as boron nitride, MoS_2, and graphene.[60]

Liquid-phase exfoliation techniques aim to achieve controlled thinning of nanoscale 2D materials by employing ionic liquids, surfactants, or organic solvents. In this approach, bulk materials are separated into smaller individual units and uniformly dispersed in solvents to minimize aggregation. Typically, the procedure integrates mild ball milling with ultrasonic treatment to achieve effective exfoliation and layer reduction.[60,64]

2.2. Bottom-up methods

In bottom-up approaches, strategies such as chemical vapor deposition and wet chemical synthesis are commonly employed to fabricate single-layered materials. These methods have attracted significant attention because they are easy to perform and highly reproducible, often enabling the synthesis of materials with diameters up to 10 nm.[57,65] The most effective technique for depositing thin films or inorganic materials on high-purity substrates is chemical vapor deposition (CVD).[66] CVD provides precise control over the dimensions and physical properties of the grown materials. On the other hand, wet-

Table 1 Different synthesis methods

Sl. no.	Material	Method	Applications	Ref.
1	$MgFe_2O_4$/rGO	Bottom-up	Removal of methylene blue (MB) dye	69
2	CeO_2/CoAl-LDH	Bottom-up	Photocatalytic hydrogen evolution	70
3	PEGylated BP nanoparticles	Top-down	PA imaging and PTT	71
4	rGO-5FU-CMARX	Top-down	Drug delivery, melanoma skin cancer treatment	72
5	Ta_4C_3 nanosheet	Top-down	PA dual-mode imaging, PTT	73
6	Alg-DOX-Cu MOF-LDH	Bottom-up	Drug delivery	74
7	$Ca_2Fe_8O_{14}$/rGO	Bottom-up	PTT, hyperthermia applications	75
8	iRGD-modified graphene oxide nanosheet	Bottom-up	Drug delivery, PTT	76
9	Ti_3C_2@Qu nanosheet	Top-down	PTT	77
10	MoS_2/Bi_2S_3-PEG nanosheets	Bottom-up	Multimodal imaging, PTT	78

chemical synthesis is used to generate transition-metal dichalcogenides in solution, often yielding high product yields. This technique is particularly suitable for preparing 2D nanomaterials that are difficult to obtain consistently through other methods. Moreover, it enables precise control over size and physicochemical characteristics along with good reproducibility, which makes it highly advantageous for large-scale fabrication (Table 1).[64,67,68]

2.3. Surface modifications for biological applications

Tailoring and functionalizing the surfaces of 2D nanomaterials are vital for customizing treatments targeting specific diseases and improving their distribution within the body. These modifications focus on effective drug binding to enhance therapeutic outcomes. One method to accomplish this is doping, which involves adding specific impurities, such as various metal elements, to the nanomaterials.[79,80] Such impurities are introduced by adding a dopant precursor, usually in the form of a salt, prior to the nucleation stage.[57] The surface decoration technique involves applying a therapeutic agent to the surface of the 2D nanomaterial. These agents include metals, polymers, drugs, biomolecules, and radioisotopes. These surface functionalizing agents are further subcategorized into different types as depicted in Fig. 1. The agents can be added using either top-down or bottom-up methods through chemical bonding, physical adsorption, and various interactions, including hydrophobic and electrostatic forces.[64]

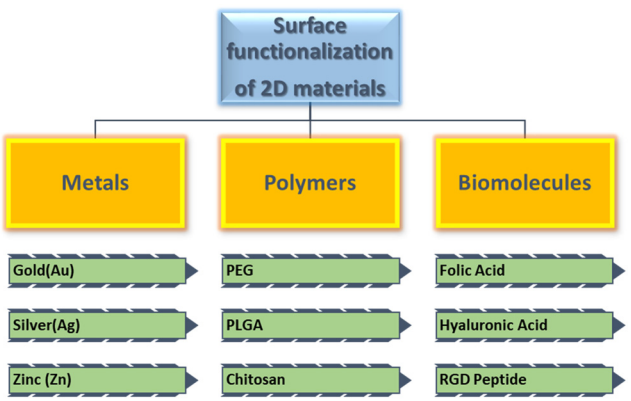

Fig. 1 Classification of different types of surface modifications used in 2D nanomaterials.

3. Common types of 2D nanoparticles

3.1. Graphene and its derivatives

Since Novoselov and Geim isolated graphene in 2004 using the adhesive tape method and characterized its unique structure and electronic properties, the development of graphene-based 2D nanomedicines has advanced significantly.[81] Graphene-related materials encompass a variety of compounds with unique characteristics. These include different derivatives, including graphene oxide (GO), reduced graphene oxide (rGO), evolving as 2D nanomaterials like graphydine (GDY), and nano graphene oxide (NGO). GO is composed of a single layer of carbon atoms placed in an sp^2-hybridized structure, decorated using various oxygen-containing functional groups, making it highly versatile for applications, particularly in nanomedicine.[7,8,10] The graphene sheets are bound together by weaker forces such as van der Waals interactions, while their edges contain reactive sites, delocalized π–π electrons, and aromatic structures. These characteristics make graphene highly suitable for biosensing and adsorption applications.[82] In graphene, individual layers are separated by approximately 3.35 Å and in a single layer, the carbon–carbon bond length is about 1.42 Å. These structural properties allow graphene to be synthesized in diverse sizes and forms using techniques such as redox processes, liquid-phase and chemical vapor deposition (CVD), epitaxial growth on silicon carbide (SiC), and mechanical exfoliation.[83]

Graphene possesses a range of impressive biological properties, including strong photothermal effects, enzyme-mimicking behavior, and substantial drug-loading capacity as well as antibacterial and anti-tumor activities (Fig. 2).[20,76,84–86] In addition, its excellent electrical conductivity, mechanical strength, optical transparency, and atomic thinness make it a subject of extensive research. Scientists are actively exploring graphene-based biosensors for detecting various biomolecules.[87–89] In the field of cancer theranostics, nanographene with various surface modifications is being studied for its potential to deliver therapeutic agents directly into cells, particularly during PTT, with promising results in both laboratory and clinical investigations.[90]

Graphene-based nanomaterials demonstrate a high efficiency in converting absorbed light into heat through

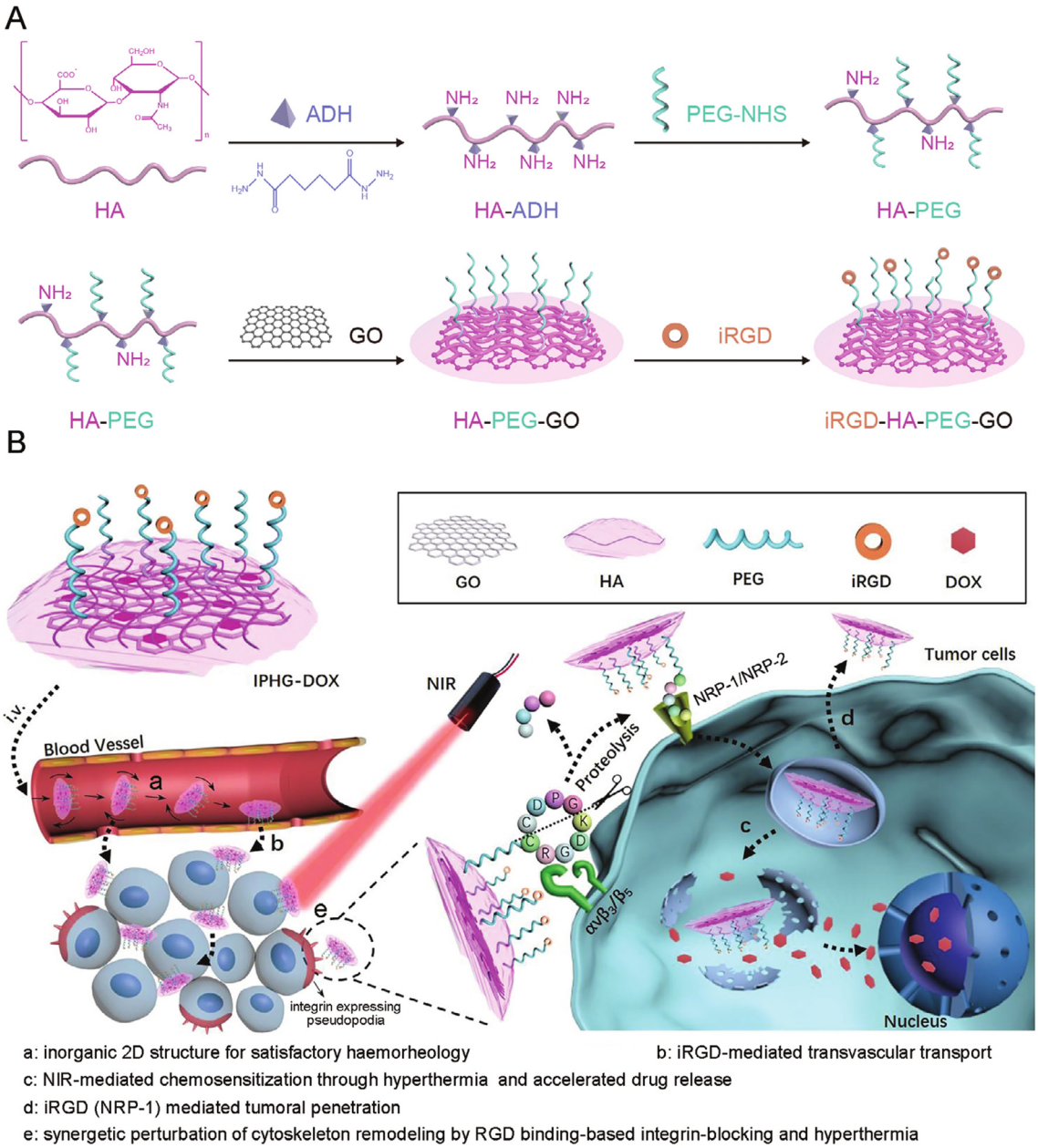

Fig. 2 (a) Schematic illustration of the fabrication of IPHG-DOX. (b) Depiction of its tumor targeted penetration and NIR-induced chemosensitization, driven by PTT-regulated drug release, heat stress induction, integrin-specific targeting, and the combined PTT-mediated inhibition of tumor cell migration. Adapted from ref. 76 with permission from Wiley Advanced [H. Wang, J. Zhou, Y. Fu *et al.*, *Adv. Healthcare Mater.*, 2021, **10**, 2100536], copyright 2021.

photothermal conversion. They are particularly effective in the NIR region, known as the biological tissue transparency window, thereby enabling localized deep-tissue hyperthermia.[91] This localized heating can be used in PTT to eliminate cancer cells in a minimally invasive manner. Additionally, the nanoscale size of graphene-derived nanomaterials enhances their permeability, retention, and preferential accumulation at tumor sites.[92]

Graphene-based systems have also been highly modified with various diagnostic and therapeutic properties, taking into account these built-in photothermal and target agents. Hatamie and colleagues developed GO/cobalt nanocomposites with dual functionality for magnetic fluid hyperthermia and magnetic resonance imaging applications. These nanocomposites were prepared *via* a chemical synthesis route, in which GO served as the base material for the assembly of cobalt nanoparticles averaging 15 nm in size, with cobalt accounting for about 80% of the total composition. Hyperthermia tests demonstrated that the dispersions exhibited efficient electromagnetic-to-thermal energy conversion at 350 kHz, particularly at concentrations of 0.01 g L^{-1} and 0.005 g L^{-1}. Furthermore, MRI studies demonstrated that the negatively charged GO/cobalt

nanocomposites significantly improved the contrast in T1-weighted imaging.[93] Extending this multifunctional approach, Lamb and colleagues developed graphene nanoflakes (GNFs) functionalized with various groups, serving as a theranostic platform. The modifications comprised a peptide ligand Glu-NH-C(O)NH-Lys targeting the prostate-specific membrane antigen (PSMA), the antimitotic agent (*R*)-ispinesib, the chelating agent desferrioxamine B (DFO), and an albumin-binding moiety to prolong circulation time *in vivo*. To evaluate their diagnostic and therapeutic performance, these conjugates were radiolabeled with ^{68}Ga and examined through both *in vitro* and *in vivo* experiments.[94]

Similarly, Baktash *et al.* created a hybrid theranostic nanosystem by combining Fe_3O_4 magnetic nanoparticles with chitosan-grafted GO as a pH-sensitive carrier. High molecular weight chitosan improved DOX loading and controlled release, while hydrophobic chitosan enhanced MRI contrast, achieving an r_2/r_1 value of 28.95 compared to 6.37 for Fe_3O_4/GO and 14.66 for Fe_3O_4. The system was biocompatible with L929 fibroblasts and, when loaded with DOX, demonstrated stronger anticancer activity against MCF-7 cells (39% viability) than free DOX (53%).[95] A GO/$MnWO_4$/PEG nanoplatform was synthesized *via in situ* growth of $MnWO_4$ on GO, yielding enhanced NIR absorption, superior photothermal conversion, and strong PA imaging performance. It exhibited high longitudinal relaxitivity (r_1 = 11.34 Mm^{-1} S^{-1}), making it a powerful dual MRI/PA contrast agent. The system also showed high DOX loading (550 mg g^{-1}) and, under laser irradiation, achieved ~90% cancer cell death, compared with 50% with free DOX.[96]

Complementing these developments, Cheng *et al.* introduced a gentle thermal annealing technique to induce blue fluorescence in GO suspensions while preserving the oxygen-containing groups essential for drug attachment. This method yielded a biocompatible, non-toxic nanomaterial that functions dually as a cellular imaging agent and drug carrier in CT26 cancer cells, eliminating the need for external fluorescent tags. Furthermore, GO was covalently linked to cisplatin, and the annealed GO notably enhanced the anticancer activity of cisplatin against CT26 cells.[97]

3.2. TMD

Transition metal dichalcogenides are a category of 2D layered materials with the typical formula MX_2, where M is a transition metal such as molybdenum, tungsten, or titanium, and X is a chalcogen such as sulfur, selenium, or tellurium.[98] These materials are composed of layers, with each sheet consisting of a metal-atom layer sandwiched between two layers of chalcogen atoms. The atoms are bonded covalently within each sheet, while weak van der Waals forces hold the adjacent layers together.[99]

Due to their layered architecture, transition metal dichalcogenides can be peeled into a single or a few-layer nanosheet, much like graphene. Certain TMDs, such as MoS_2, show in-plane anisotropy and flexibility in specific crystallographic phases like the 1T phase (Fig. 3).[100] A notable feature of many TMDs is their semiconducting property, having band gaps usually between 1 and 2 eV. The bandgap often widens as the number of layers decreases, and in some cases, such as with molybdenum- or tungsten-based TMDs, it shifts from indirect in bulk form to direct in monolayer form.[101] This tunability of the bandgap enhances their excellent optoelectronic performance, allowing absorption and emission across ultraviolet, visible, near-infrared, and far-infrared

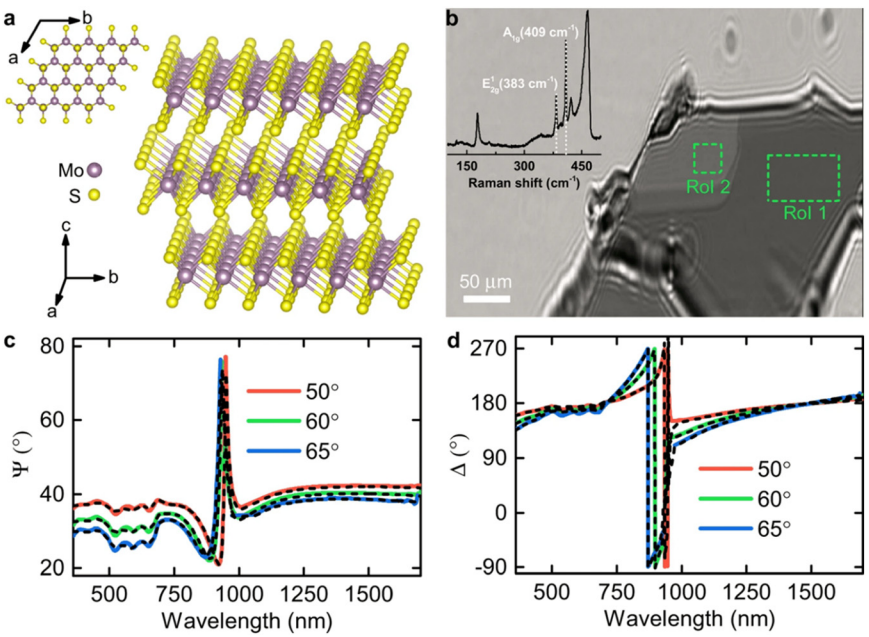

Fig. 3 (a) Structure of MoS_2 showing strong intralayer and weak interlayer bonding, causing high anisotropy. (b) Ellipsometer image of MoS_2 on 285 nm SiO_2/Si; inset Raman spectrum confirms 2H phase. (c and d) Ellipsometric ψ and Δ showing ~900 nm interference peak from SiO_2, evidence of strong anisotropy. Reproduced from ref. 100 with permission from Nature [G. A. Ermolaev *et al.*, *Nat. Commun.*, 2021, **12**, 854.], copyright 2021.

regions. TMD nanosheets are made using various methods, including chemical vapor deposition (CVD), mechanical and liquid-phase exfoliation, and laser thinning. These techniques aim to overcome the interlayer van der Waals forces to isolate thin nanosheets. For example, single-layer MoS_2 and WSe_2 nanosheets produced by mechanical exfoliation have been successfully used in the fabrication of field-effect transistors.[102]

Owing to their exceptional electronic and optical properties, 2D TMDs have emerged as promising materials in biomedical applications such as biosensing, imaging, and phototherapy. In one notable example, a composite film of MoS_2 and poly(lactic-*co*-glycolic acid) (PLGA) was integrated onto a 3D-printed bioactive glass scaffold. This multifunctional platform both demonstrated tumor-suppressing capabilities *via* PTT against osteosarcoma cells and facilitated bone generation by promoting the proliferation and differentiation of rat bone mesenchymal stem cells (rBMSCs).[103]

3.3. MXenes

Amongst the 2D nanomaterials, MXenes are a rapidly expanding group of 2D materials primarily composed of transition metal carbides, nitrides, or carbonitrides, with the general formula $M_n + 1X_n$ (where n = 1–4, M is a transition metal such as molybdenum, niobium, or titanium, and X is carbon or nitrogen). Since their initial discovery as Ti_3C_2 in 2011, more than 20 distinct MXenes have been experimentally produced, while theoretical studies suggest the possibility of over 70 additional variants, making them one of the most prominent known families of 2D materials.

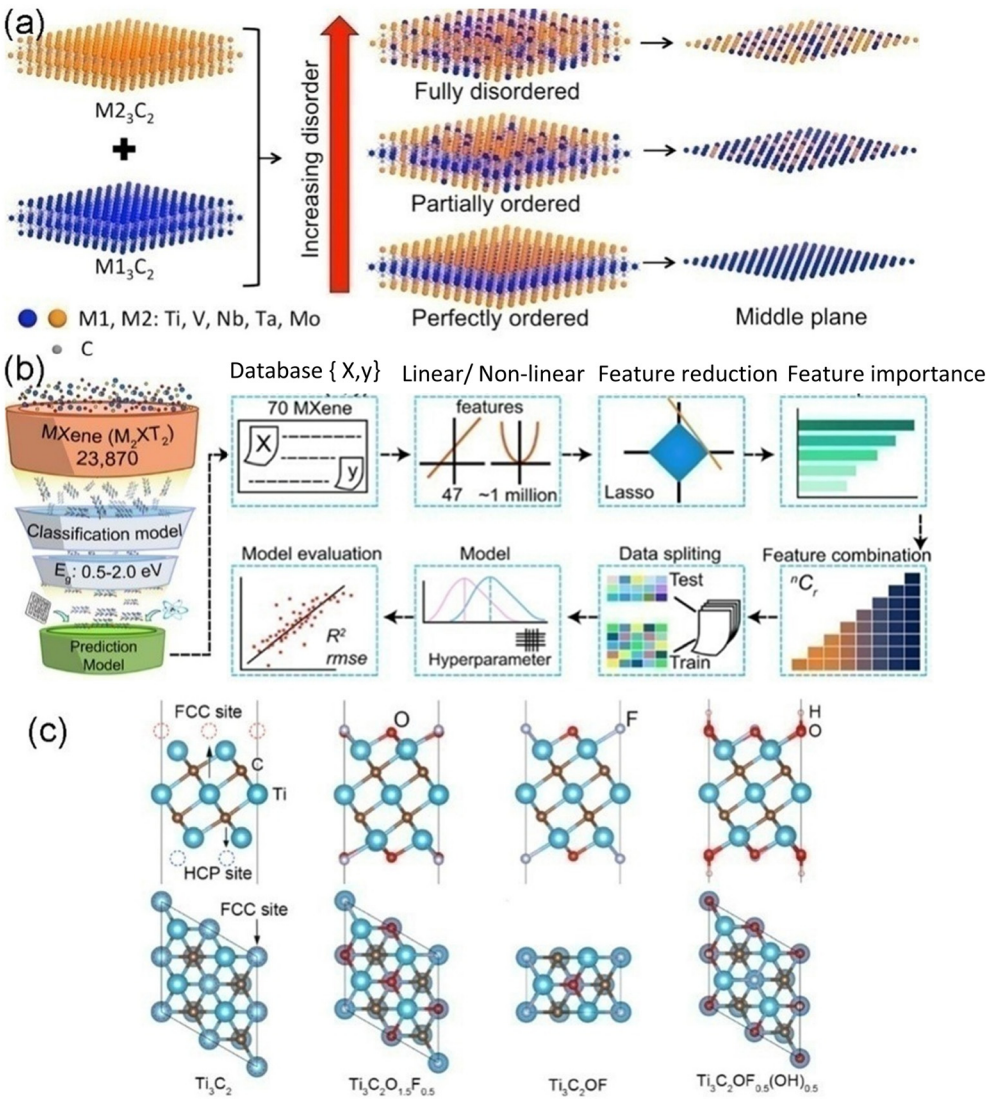

Fig. 4 (a) Figure illustrating the creation of MXene alloys. M1 and M2 represent transition metals such as Ti, V, Nb, Ta and Mo. Adapted from ref. 106 with permission from ACS [T. L. Tan, H. M. Jin, M. B. Sullivan, B. Anasori and Y. Gogotsi, *ACS Nano*, 2017, **11**, 4407–4418], copyright 2017. (b) Schematic illustration of the process of selecting semiconductor materials from the MXene database using machine learning techniques. Adapted from ref. 107 with permission from ACS [A. C. Rajan, A. Mishra, S. Satsangi, R. Vaish, H. Mizuseki, K.-R. Lee and A. K. Singh, *Chem. Mater.*, 2018, **30**, 4031–4038.], copyright 2018. (c) O-containing $Ti_3C_2T_x$ MXenes are the most stable. Adapted from ref. 108 with permission from ACS [T. Hu, M. Hu, B. Gao, W. Li and X. Wang, *J. Phys. Chem. C*, 2018, **122**, 18501–18509], copyright 2018.

Their unique combination of metallic conductivity, hydrophilicity, and tunable surface chemistry has led to diverse applications in energy storage, biomedical devices, environmental remediation, and advanced electronics.[31] MXenes commonly feature a layered structure represented by the formula $[MX]_nM$, which means that (n) layers of carbon or nitrogen (X) are sandwiched between (n + 1) layers of a transition metal (M). When only a single layer is present, these MXenes are known as monolayers and are typically less than 1 nm thick, reflecting their minimal atomic thickness. In contrast, multilayer MXenes are composed of multiple stacked layers that can vary in thickness from several nm to mm, depending on their preparation. Moreover, the distinctive way MXenes are synthesized often leaves their surfaces covered with a variety of functional groups, including fluorine, oxygen, and hydroxyl groups.[104]

Like other 2D materials, MXenes can be synthesized using well-established top-down exfoliation strategies. The chosen technique often varies depending on the precursor material, the composition of the etchant, or the type of intercalating agent used. Of these methods, etching remains the predominant approach for fabricating ultrathin MXene nanosheets. Etching techniques are generally categorized into high-frequency and low-frequency processes, with a mixture of hydrofluoric acid (HF) and tetrapropylammonium hydroxide (TPAOH) being a particularly popular combination for both etching and exfoliating MXene layers (Fig. 4).[31,105–108]

MXene's distinctive layered structure and chemical formula enable it to combine the high electrical conductivity typical of transition-metal carbides or nitrides with the surface hydrophilicity imparted by its functional groups. This dual property endows MXenes with remarkable capabilities in both photoelectric and magneto-electric applications.[18] MXenes' metallic components primarily govern their electrical conductivity and magnetic behavior, while surface functional groups that can donate electrons substantially modulate these properties. The materials' luminescent properties are critically influenced by nanoscale size effects, including quantum confinement phenomena and light emission arising from structural defects. MXenes' well-defined ordered atomic arrangement enables accurate prediction and analysis of these properties through advanced computational modeling techniques.[31] In recent years, 2D nanomaterials, such as MXenes, have emerged as promising candidates for biomedical applications. Their nanometer-scale dimensions help extend their presence in the bloodstream while also unlocking new capabilities, such as efficient binding and light emission.[18]

The aforementioned inherent physicochemical properties have provided the basis for 2D nano-MXenes, which represent a highly promising option for the accurate diagnosis and targeted therapy of malignant diseases. Moreover, their suitability for biomedical use is enhanced by several distinctive advantages: (i) hydrophilic surface groups such as hydroxyl, oxygen, or fluorine, enhances their biomedical utility; (ii) their easy composition, incorporating biologically essential elements like carbon and nitrogen alongside biocompatible transition metals like titanium, niobium, and tantalum which supports excellent compatibility with living tissues and enables controlled breakdown within the body; (iii) MXenes display strong absorption in the NIR region, making them valuable for near-infrared photoacoustic imaging (PAI) and PTT across both NIR-I and NIR-II spectral ranges.[109]

3.4. Nanoclay/LDH

Clay nanomaterials are drawing growing interest because of their distinctive physical and chemical properties. Their unique physical structure, like their thin-layered architecture, endows them with remarkable qualities, especially due to their inherent surface charges. Since medieval times, clay-based substances have been commonly utilized in food and nutrition. Due to the emerging nanotechnology, clay nanomaterials are finding various applications, including healthcare products, cosmetics, and biomedical fields. In biomedicine, these materials are drawing attention due to their efficient biological properties.[110] Clay is naturally occurring and mainly composed of fine-grained phyllosilicate minerals. These minerals are composed of a variety of elements and exist in different particle sizes, forming stacked, sheet-like structures.[111] Clays consist mainly of octahedral and tetrahedral structural units. These units can be combined in different arrangements and compositions, resulting in unique clay types such as palygorskite–sepiolite, smectite (or bentonite), and kaolinite.[112]

The composition and characteristics of natural clays differ considerably based on their geographic sources. Although this variety broadens the selection of clay materials, it can restrict their suitability for biological uses. Consequently, synthetic mineral clays have gained interest in biomedical applications, as they provide consistent properties and composition and can be manufactured in substantial amounts with greater ease. Synthetic mineral clays, engineered with tunable biological activity, provide a reliable solution to the variability and unpredictability of natural clays (Fig. 5).[113,114] Hydrotalcite (LDH), is a synthetic clay that has attracted growing interest in recent years. It features stacked layers that resemble brucite, with positively charged layers and negatively charged anions between them. Although hydrotalcite is rare in nature, it is widely utilized in various fields due to its adaptable properties.[115] The surface charge ratio $X = M^{3+}/(M^{2+} + M^{3+})$ depends on the relative proportions of the two metal ions and can be adjusted for specific uses. However, many lamellar LDH flakes tend to cluster, reducing their effectiveness. By exfoliating bulk LDHs into single-layer nanosheets, their performance is enhanced due to the increased specific surface area and unique characteristics of each layer. These monolayer nanosheets are not only important for fundamental studies but also serve as a versatile base for fabricating advanced functional nanomaterials.[116]

A popular method for using monolayer nanosheets (NSs) is the wet-chemical approach, which involves layer-by-layer assembly with a compatible charged material. This highlights the essential role of monolayer NSs. Furthermore, several

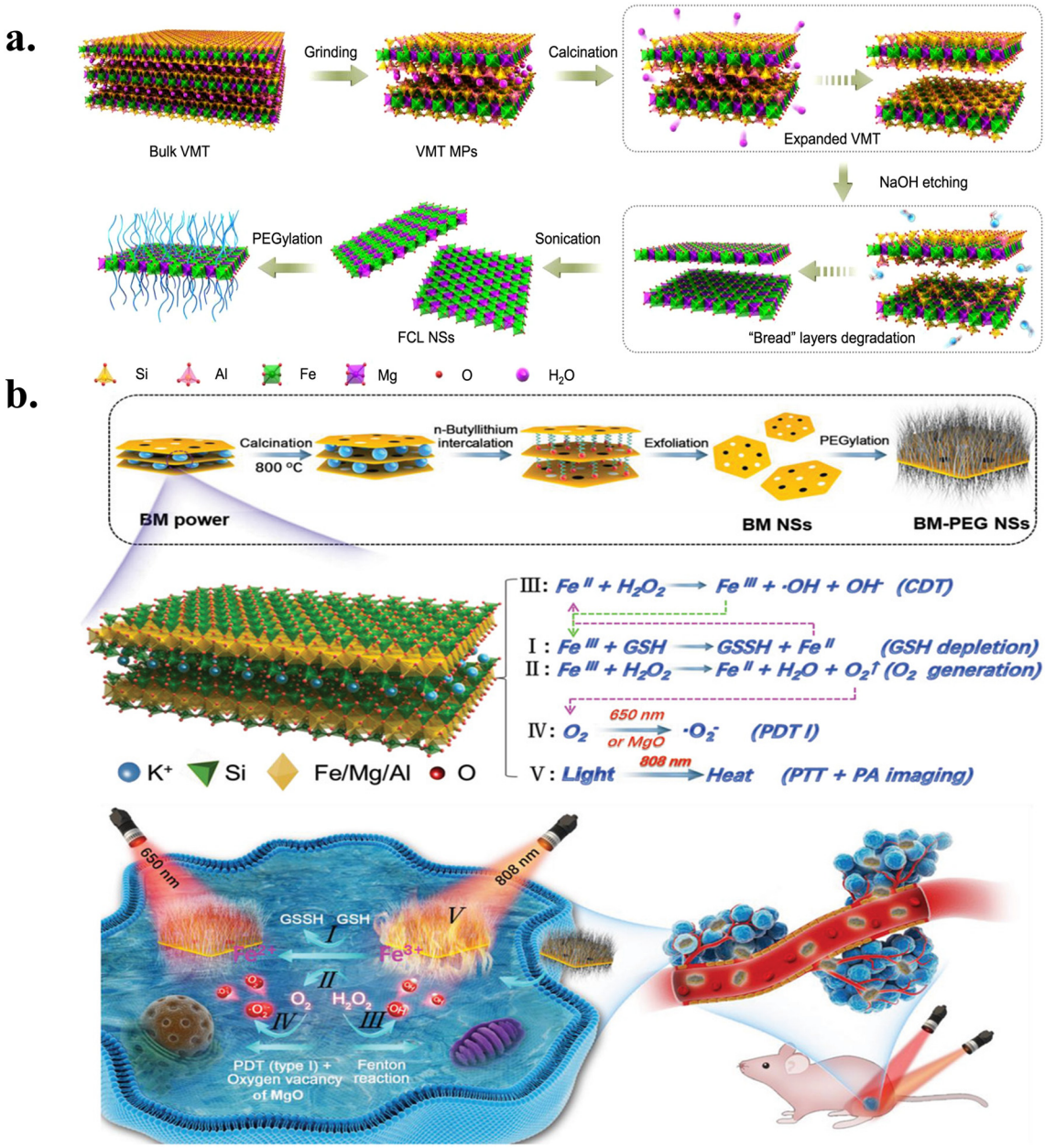

Fig. 5 (a) Schematic diagram showing the preparation of FCL-PEG NSs, reproduced from ref. 113 with permission from *Nature Communications* [X. Ji *et al.*, *Nat. Commun.*, 2021, **12**, 1124], copyright 2021. (b) Preparation process of BM-PEG-NSs and the mechanism by which they perform PTT, reproduced from ref. 114 with permission from *Advanced Science* [X. Ji *et al.*, *Adv. Sci.*, 2019, **6**, 1901211], copyright 2019.

techniques have been created to manufacture LDHs, mainly through top-down exfoliation and bottom-up synthesis.[117] The bottom-up synthesis approach involves producing specific nanosheets directly from precursor materials in a single step. In contrast, the exfoliation process for layered materials generally proceeds in two stages: first, the insertion of an intercalating agent to expand the interlayer spacing, followed by the separation of the layers. The choice of intercalating agent affects both the efficiency and the yield of LDH nanosheets that are widely used in biomedical applications. The distinctive physicochemical properties of LDH nanosheets make them particularly well suited for biomedical applications.[117]

4. Advancements of 2D nanoparticles in cancer theranostics

2D nanomaterials like graphene, TMDs, MXenes, h-BN, and BP exhibit promising potential in revolutionizing the field of cancer theranostics, where drug delivery and diagnosis can be combined using imaging modalities.[118] The unique properties of these materials, such as their atomically thin nature, ultra-high surface area, and optical and electronic properties that can be controlled by surface functionalization, make them suitable for drug loading, targeted ligand molecules, and imaging probes in the same particle.[119] Such

Table 2 Summary of 2D nanomaterials for cancer theranostics

Sl. no.	2D nanomaterials	Targeted disease	Performance	Ref.
1	MoS_2-PEG–biotin–Cur/Er	Lung cancer (A549)	~95% tumor growth inhibition ratio (*in vivo*)	125
2	AAP10-pDA/rGO	Breast cancer	~100% tumor growth inhibition ratio	126
3	Gold–BP nanosheets	Lung cancer (A549)	~100% complete tumor growth suppression	127
4	GO-aptamer sensor	Prostate cancer (PSA detection)	~95% sensitivity rate	128
5	Chitosan/HA/BP/scaffold	Osteosarcoma (bone cancer)	~95% cancer cell elimination rate	129
6	MoS_2-HPG	Multi-drug resistant cancer	88.9% loading efficiency	130
7	PAMAM–GO	Lung cancer (CD47 siRNA delivery)	80% success rate	131
8	BP nanosheets-C60	Breast cancer (4T1)	90% *in vitro* inhibition rate	132
9	PEGylated GO (DOX loaded)	Breast cancer	72% tumor growth inhibition	133
10	FA–GO + miR-124	Glioblastoma (brain tumor)	30% increase in survival rate	134

potential has been utilized in the diagnosis and treatment of certain cancers like breast cancer, lung cancer, prostate cancer, and brain tumors. Graphene-based nanocarriers have been intensively investigated for targeted drug delivery and PTT in breast cancer. During photothermal therapy, 2D materials like graphene nanosheets and MXenes show excellent NIR absorption, leading to local tumor ablation with minimal harm to surrounding tissues. This method has worked especially well for treating breast and skin cancer.[120,121] Additionally, they have been used in combination with PDT, where ROS generation is induced by light exposure, thereby improving the anticancer potential, mostly for lung and cervical cancer.[122] Furthermore, black phosphorus nanosheets have also demonstrated great efficacy in the treatment of glioblastoma due to their biodegradability and efficient photothermal conversion.[28]

In the field of diagnostic imaging techniques, these materials have shown the property of photoluminescence, SERS effect, and ability to act as contrast agents for MRI, CT, and photoacoustic imaging. These properties make it possible to find and keep an eye on tumors early, such as liver cancer and pancreatic cancer, where early diagnosis is very difficult.[123] New advancements have been made to ensure that stimuli-responsive 2D structures, such as those activated by pH changes, redox conditions, or NIR radiation, can be used for the selective delivery of drugs to the tumor microenvironment, thereby minimizing any form of side effects. These systems enable targeted drug release within the tumor microenvironment, enhancing therapeutic efficacy while reducing systemic toxicity in malignancies such as colorectal and ovarian cancer.[124] Overall, 2D nanomaterials offer great promise for future cancer theranostics (Table 2).

4.1. Photothermal therapy

Photothermal therapy (PTT) uses light-absorbing agents that interact with electromagnetic radiation, usually in the infrared range, to treat tumors and other diseases. When these agents absorb light, their electrons are excited to a higher energy level. As they return to a lower energy state through non-radiative processes, heat is produced, increasing the temperature in the surrounding tissue.[135,136] Melamed *et al.* studied the mechanism of PTT-induced cell death and reported that the cell death is primarily caused by apoptosis rather than necrosis, thereby reducing inflammatory side effects.[137] Pérez-Hernández *et al.* investigated PTT-based apoptosis pathways and observed that under low-energy light exposure, the intrinsic pathway is the primary mechanism responsible for PTT-induced apoptosis.[138] Supporting this, they found decreased Bid levels and increased tBid expression after PTT, as shown by western blot analysis. Flow cytometry results demonstrated a loss of mitochondrial membrane potential following treatment, and caspase-3 activation was also observed. These findings indicate that PTT effectively triggers apoptosis through the intrinsic pathway under proper therapeutic conditions.[137]

4.1.1. Graphene-based nanomaterials in PTT. Graphene oxide (GO) and reduced graphene oxide (rGO) are the main forms of graphene-based nanomaterials within the larger group of carbon nanomaterials.[139–141] Nanographene is being investigated as a PTT system to improve therapeutic performance for cancer treatment. Both GO and rGO types exhibit excellent biocompatibility and unique structural features, making them highly suitable for a range of biomedical uses.[142]

Graphene has attracted significant research interest because of its excellent electrical conductivity, high tensile strength, transparency, and ultra-thin nature.[87–89] These inherent characteristics further enhance the exceptional photothermal efficacy of graphene-related materials, which are especially effective at absorbing light energy and converting it into heat, a property that makes them ideal for PTT. This heating effect results in the breaking of non-covalent bonds triggered by increased temperature during NIR laser exposure.[143] Furthermore, structural modifications are crucial for enhancing GO's effectiveness in PTT. This involves incorporating carboxyl (–COOH) and hydroxyl (–OH) groups at the material's edges, while carbonyl (C═O) and epoxy (–O–) functional groups can be strategically placed on its basal plane. These adjustments optimize GO's properties, facilitating its structural development for targeted PTT applications.[144] GO offers hydrophilic surface rich in reactive groups, making it highly adaptable for attaching a diverse range of substances used in PTT.[145,146] Although graphene nanomaterials have a nanosheet morphology and a large surface area, their photothermal efficacy is limited without functionalization, which can be enhanced by incorporating polymeric materials.

Expanding on these modifications, specifically engineered GO nanosheets are used in cancer treatments involving hyperthermia to examine their effects on macrophage and lymphocyte activity. PEGylated GO nanosheets (1-GOs and 6-GOs), developed specifically for hyperthermic cancer treatment, exhibited an interesting but highly selective immune response. The study reported that although 6-GOs caused an increase in TNF-α production by LPS-activated macrophages without causing a general disruption in IL-6 or IL-1β levels, both types inhibited lymphocyte proliferation and IL-6 release in splenocytes, which is certainly helpful but poses a serious problem in terms of whether such inhibition is a reflection of biocompatibility or rather cytotoxic interference with the immune system's surveillance process. Furthermore, the difference in responses seen between RAW-264.7 macrophages and splenocytes clearly indicated another issue, namely that immortalized cell lines cannot be considered a reliable basis for assessing biocompatibility due to their inherent deviation from *in vivo* conditions. The classification of these mild inflammatory responses as advantageous for cancer treatment is thus premature in the absence of long-term *in vivo* data differentiating between temporary immune regulation and immunosuppression.[147]

Additionally, the therapeutic efficacy of nanomaterial-based photothermal systems must be interpreted cautiously, even when short-term outcomes appear promising. For instance, the NAu–rGO composite was reported to be highly efficient in NIR-mediated PTT, achieving swift heating of the surroundings up to 49 °C *via* 800 nm laser exposure (0.5 W cm^{-2}, 5 min) at 10 μg mL^{-1}, superior to rGO (25 °C) and AuNPs (38 °C) due to the combined plasmonic heating properties of AuNPs (polydispersed from 5 to 30 nm) and

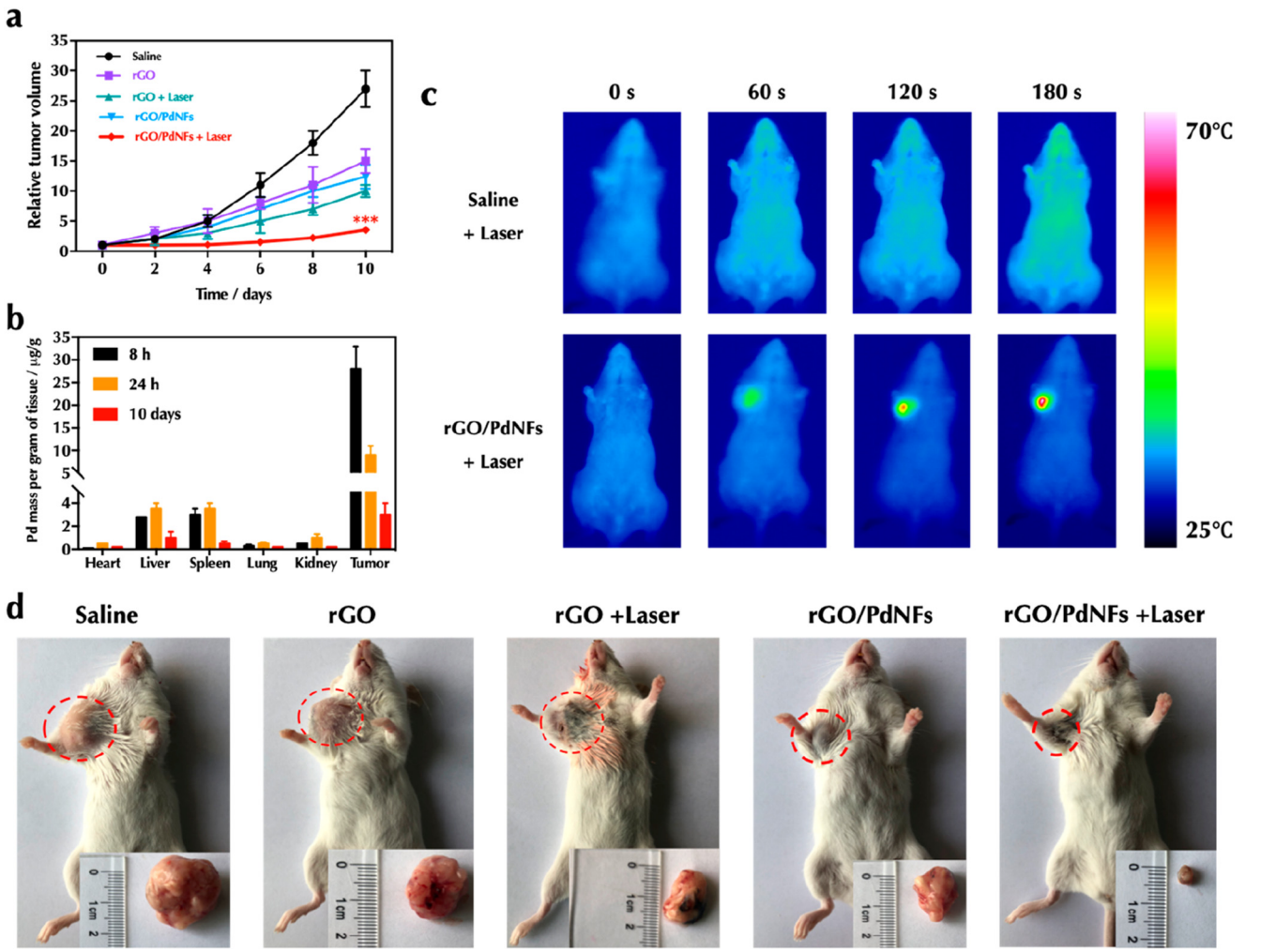

Fig. 6 Photothermal therapy on tumor *via* rGO/PdNFs *in vivo*. (a) Tumor growth rate in mice under different conditions of treatment. (b) Biodistribution study of rGO/PdNFs in tumor-bearing mice, which were administered rGO/PdNFs for specific time points. The biodistribution of rGO/PdNFs in organs and tumors of mice was confirmed through the measurement of the level of Pd using ICP-MS technique. (c) Infrared images of tumors in tumor-bearing mice that had been injected with saline or rGO/PdNFs and then illuminated using a laser (1.5 W cm^{-2} for 3 min). (d) Photographs of tumor-bearing mice and extracted tumors after 10 days of treatment. $^{*}P < 0.05$, $^{**}P < 0.01$, $^{***}P < 0.001$ compared with the saline group. Reproduced from ref. 150 with permission from ACS [Y. He, W. Cao, C. Cong, X. Zhang, L. Luo, L. Li, H. Cui and D. Gao, *ACS Sustainable Chem. Eng.*, 2019, **7**, 3584–3592], copyright 2019.

increased thermal conductivity of rGO. The hyperthermia resulted in an approximately 80% cell death rate of MCF-7 breast carcinoma cells after 24 hours, supported by MTT testing and live/dead confocal analysis, revealing prevalent red (dead) over green (live) fluorescent images.[148] The mechanism of action in NIR-PTT is based on the absorption of the 808 nm wavelength light by the rGO–Ru–PEG nanoparticles with high efficiency due to high rGO NIR absorbance and efficient conversion into heat energy, which resulted in the increase in temperature from room temperature to up to 33 °C (solution 10 μg mL^{-1}, 10 min), followed by lysosomal damage, increased concentration of reactive oxygen species (ROS) due to an additional synergic PDT effect in 450 nm irradiation, activating caspase-3/7 and reducing ATP levels, ultimately leading to apoptosis in A549 cancer cells (37.5% annexin V positive). At a laser power density of 0.5 W cm^{-2}, tumors could reach 58.7 °C in 5 min, providing imaging guided PTT–PDT with high therapeutic potential. The rGO–Ru–PEG complex shows pH-sensitivity (faster release at pH 5) and laser-induced Ru–PEG release.[149]

Furthermore, the physicochemical characteristics of the material itself become equally important. The synthesis of the $Ca_2Fe_8O_{14}$/rGO composites by auto-combustion using the sol–gel method and conventional ceramic procedures produced a structure that exhibits a gradual reduction in lattice parameters along with varying crystallite sizes with increasing content of hexaferrites due to the disruptive effect of rGO on the process of crystal formation. Despite the negative correlation between the amount of rGO used and coercivity, coupled with increased magnetization, indicating suitability for soft-magnetic applications, the low specific absorption rate (SAR) raises an important question about its effectiveness, as clinically successful magnetic hyperthermia therapy requires a higher SAR to reach the required heating temperature range of 42–45 °C. However, the wide range absorption of NIR light and photoluminescence attributed to oxygen vacancies make the material a promising multimodal candidate for photothermal and magnetic hyperthermia treatment methods.[75]

In another study, rGO/PdNFs were proposed as a novel multifunctional nanosystem with applications in ethanol oxidation, nonenzymatic glucose detection, and photothermal tumor treatment owing to their high-efficiency flower-like palladium structure in terms of catalysis and photothermal conversion. The developed nanomaterial exhibited remarkable photothermal effect (up to ~70 °C), excellent cell uptake capacity and minimal cytotoxicity while inducing up to ~80% death of cancer cells under illumination by laser light *in vitro*. Moreover, the nanomaterial facilitated fast tumor temperature increase (~65 °C) as well as tumor inhibition *in vivo*. The biodistribution studies showed efficient tumor distribution and elimination of the nanomaterial, while the results from biochemical analysis, immunological tests, and histological staining proved the lack of any adverse effect in the body systems (Fig. 6).[150]

4.1.2. MXenes in PTT. The photothermal conversion ability of nanomaterials refers to their capacity to absorb light energy and transform it into heat. This ability is mainly influenced by factors such as the material's inherent molecular or crystal structure, interactions between individual particles, coupling within the particles, and electron arrangement. The efficiency and effectiveness of this conversion process depend on how these factors influence light absorption and the subsequent thermal energy generation.[151] Generally, 2D MXenes offer significant advantages in photothermal conversion because of their large surface area, free electrons, and strong absorption across a broad range of the solar spectrum.[152] Although research on the photothermal properties of MXenes started only recently, numerous pioneering studies have been conducted to explore the fundamental mechanisms involved. For targeted photothermal therapy (PTT), MXenes are frequently modified or loaded into biocompatible carriers, such as polymers or targeting ligands, to ensure that they are accumulated selectively inside the tumors. Once the MXenes arrive at the tumor site, their activity is stimulated by NIR light, leading to LSPR in the MXene particles, which convert light into heat energy and destroy the cancerous cells.[153,154]

Owing to their intrinsic characteristics, MXenes and related materials excel in absorbing light energy due to their strong electromagnetic wave absorption capabilities, which are critical for their photothermal behavior and effectiveness as photothermal materials.[155] Shahzad *et al.* first observed multiple internal reflections in $Ti_3C_2T_x$ flakes, which help them absorb and dissipate incoming energy efficiently. The high carrier concentration on the MXene surface causes partial reflection of incident electromagnetic waves. Moreover, local dipoles generated by surface functional groups enhance the absorption of light that penetrates the $Ti_3C_2T_x$ structure. A significant amount of electromagnetic radiation enters the lattice and reflects multiple times between layers. As the waves lose energy and pass through additional MXene flakes, the cycle of reflection and absorption continues, progressively attenuating the energy. This process of penetration, reflection, and absorption gradually converts electromagnetic energy into heat.[32]

Beyond multiple scattering effects, the localized surface plasmon resonance (LSPR) effect plays a crucial role in the photothermal mechanism of MXenes by enabling surface carriers to be controlled to generate heat. Exploiting the plasmonic driven photothermal behavior, PEG/$Ti_3C_2T_x$ composite phase change materials have been developed by encapsulating PEG within ultrathin $Ti_3C_2T_x$ nanosheets, resulting in enhanced photothermal conversion and storage. This composite showed strong UV-vis NIR absorption, especially in visible and near-infrared regions, achieving a photothermal storage efficiency of 95.5%. Its high energy storage density and structural stability highlight its potential as a novel material for solar thermal energy storage (Fig. 7).[156,157] In general, materials that show LSPR, particularly metal nanoparticles, are generally beneficial for improving photothermal conversion.[158,159] When light hits the interface between metal and dielectric materials, free electrons on the metal surface oscillate collectively. This synchronized electron movement increases light absorption and plays a vital role in heat generation, which is central to the

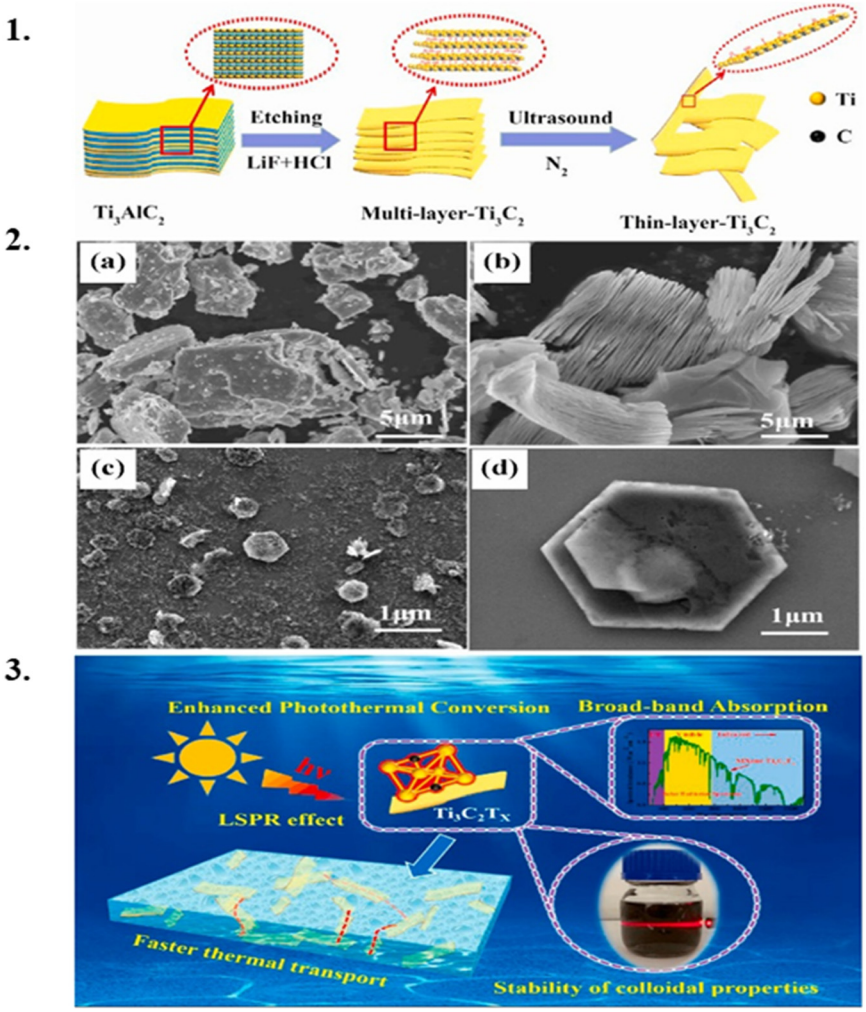

Fig. 7 (1) Preparation of multilayered $Ti_3C_2T_x$ and thin layered $Ti_3C_2T_x$ (b). (2) SEM images of (a) Ti_3AlC_2 MAX phase, (b) multilayer $Ti_3C_2T_x$, and (c and d) thin layer $Ti_3C_2T_x$. (3) The mechanism of radiation energy conversion in $Ti_3C_2T_x/H_2O$ nanofluids. Reproduced from ref. 156 with permission from Elsevier [D. B. Wang, Y. X. Fang, W. Yu, L. L. Wang, H. Q. Xie *et al.*, *Sol. Energy Mater. Sol. Cells*, 2021, **220**, 110850], copyright 2021.

material's photothermal properties.[160] The light waves couple with free electrons, producing near-field electromagnetic waves along the metal surface. Resonance occurs when electron oscillation frequencies match those of the incident light, concentrating and intensifying the electromagnetic field within a small region.[161]

Extending these fundamental plasmonic principles to MXenes, $Ti_3C_2T_x$ has been confirmed to exhibit intrinsic plasmonic behavior. MXenes, derived from the MAX phase, possess metal-like characteristics or a "semimetal" property.[162] The behavior of surface plasmons in MXenes is closely linked to the concentration of free charge carriers on their surfaces, mirroring phenomena observed in semimetals, metals, and semiconductors (Fig. 8).[77] The $M_{n+1}X_nT_x$ structure demonstrates a metallic free-electron density, a property strongly linked to its high concentration of surface terminal groups (T_x).[163] Advanced spatial analysis techniques with ultra-high precision have enabled the clear identification of MXenes' longitudinal and transverse surface plasmon oscillations as well as intrinsic interband electron transitions within their layered structures. Notably, each atomic layer in MXenes functions as an independent plane, generating distinct plasmonic resonance patterns. This behavior highlights their two-dimensional architecture and fundamental differences from conventional plasmonic metals, emphasizing the novel electromagnetic properties arising from their unique sheet-like geometry.[164]

Taking advantage of these distinctive photothermal and plasmonic properties, MXene-based systems have been increasingly explored for advanced biomedical applications. For example, a nanoplatform based on platinum-anchored V_2C MXene were engineered to combat drug-resistant bacterial infections. These nanostructures demonstrate both photothermal effects and multi-enzyme mimetic functions while also displaying outstanding biocompatibility. In laboratory and animal studies, the Pt@V_2C system effectively produces localized heat and reactive oxygen species. Its promising therapeutic results in treating conditions such as subcutaneous abscesses and bacterial keratitis suggest broad utility, extending its use to advanced catalytic and thermal treatment applications.[165]

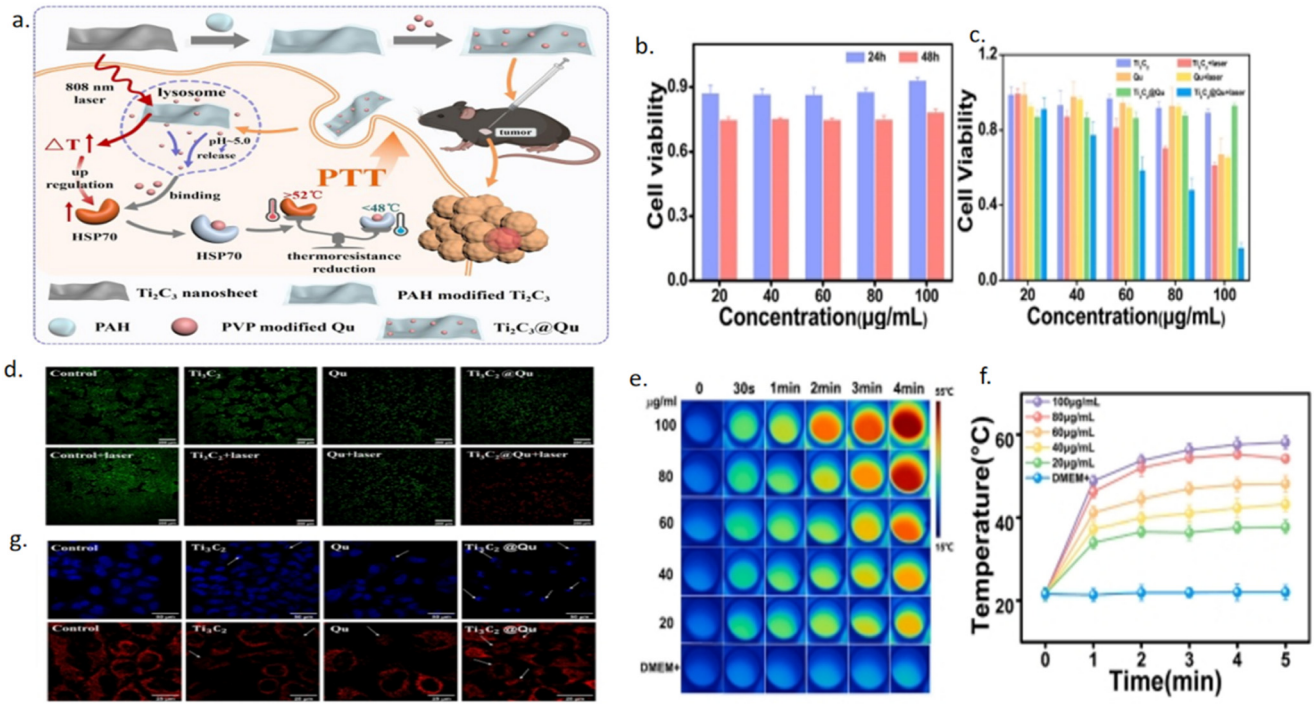

Fig. 8 (a) Schematic representation of MXenes in PTT. (b) Relative cell viability of B16 cells after culturing in different concentrations of Ti_3C_2@Qu for 24/48 h. (c) The relative survival rate of B16 cells cultivated under various treatment settings following 808 nm laser irradiation (1 Wcm^{-2}) with results expressed as mean ± SD (N = 3). (d) Confocal laser scanning microscopy (CLSM) images of B16 tumor cells after different treatment methods. (e) Infrared thermal images of different concentrations of Ti_3C_2 incubated for 6 h under 808 nm light excitation at 1 W cm^{-2}. (f) Temperature–time curves of different concentrations of Ti_3C_2 incubated for 6 h under 808 nm light excitation at 1 W cm^{-2}. (g) CLSM images of mitochondrial staining of nuclei of tumor cells after different treatment methods. Reproduced from ref. 77 with permission from Elsevier [B. Li, G. Fu, C. Liu *et al.*, *J. Colloid Interface Sci.*, 2024, **665**, 389], copyright 2024.

4.1.3. TMDs in PTT. Transition-metal dichalcogenides are considered promising photothermal contrast agents due to their pronounced near-infrared absorption and high photothermal conversion efficiency. 2D TMDs like molybdenum disulfide (MoS_2) and tungsten disulfide (WS_2) have also been found to enable multi-dimensional platforms that address the limitations of monophasic cancer therapy, capable of performing both photothermal therapy and drug delivery simultaneously.[166] It is the versatility of structure and function that has gradually prompted the use of such materials in a variety of medical applications, ranging from soft tissue tumor treatment to the much tougher area of orthopedic bone tumors, thereby making TMDs the only versatile nanoparticles in the theranostics field. Building on these multifunctional attributes, MoS_2–PLGA composites coated with borosilicate bioactive glass (BGM) were developed for the treatment of malignant bone tumors. When exposed to an 808 nm laser, BGM scaffolds exhibited rapid temperature increases with consistent photothermal performance, effectively suppressing tumor growth in animal models and reducing osteosarcoma cell survival *in vitro*. This framework also enhanced the growth and differentiation of rat bone mesenchymal stem cells, boosting expression of bone-forming genes (Runx-2, OCN, Col-I). *In vivo* experiments further demonstrate their ability to support bone regeneration in critical-sized rat defects, underscoring their potential as dual-purpose biomaterials, as shown in (Fig. 9).[167]

In line with the need to further optimize the intrinsic photothermal properties and dispersibility of TMD-based systems for such multifunctional applications, the synthesis of amphiphilic MoS_2 nanosheets ($CeMoS_2$) was reported *via* a chemical stripping method for PTT, demonstrating superior water-based dispersion compared to graphene nanosheets. These $CeMoS_2$ nanosheets, with a thickness of 1.54 nm and a size of 800 nm, exhibited an NIR absorbance of 29.2 L g^{-1} cm^{-1}, surpassing reduced graphene oxide (rGO) at 24.6 L g^{-1} cm^{-1} and significantly exceeding GO by 7.8 times. While MoS_2 nanosheets have not yet been applied in combination therapies, their properties suggest substantial potential for phototherapeutic applications. The high NIR absorbance and variability of $CeMoS_2$ highlight its promise as an effective PTT material. Transition metal dichalcogenides (TMDs), such as MoS_2, are increasingly recognized for their phototherapy prospects.[168]

4.2. Imaging

The most common imaging modalities used in cancer therapy include optical imaging (OI), magnetic resonance imaging (MRI), positron emission tomography (PET), computed tomography (CT), and photoacoustic tomography (PAT).[169] Among their most remarkable qualities are their optical

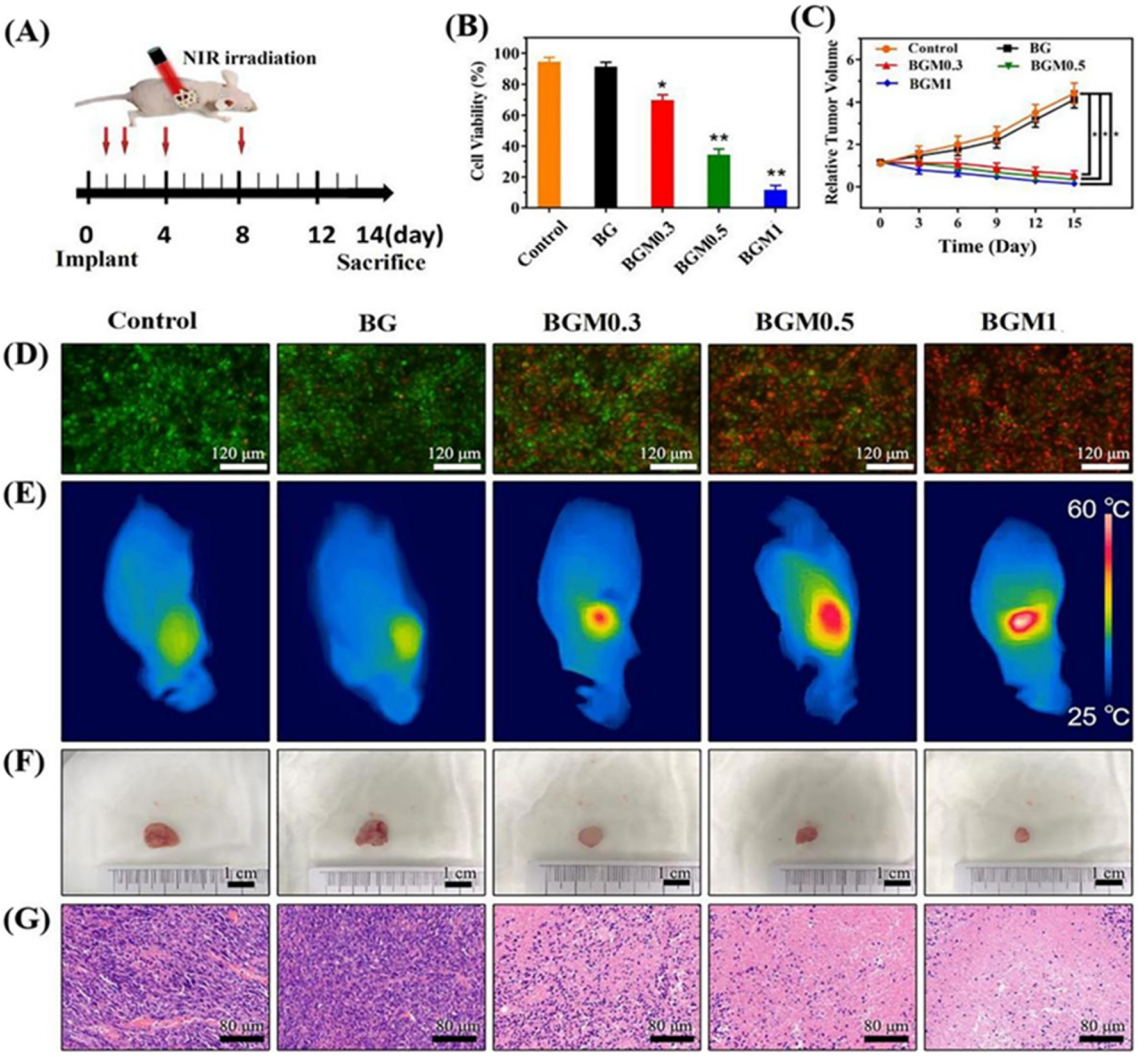

Fig. 9 (A) The photothermal therapy strategy by BGM scaffolds in a nude rat model. (B and C) Relative cell viability and tumor volume in control, BG and BGM scaffolds at day 14. (D) The live (green)/dead (red) staining of the control, BG and BGM groups. (E) Real-time NIR thermal images of BGM scaffolds under irradiation of 808 nm laser. (F) Photograph of tumors obtained from control, BG and BGM groups at day 14. (G) Representative H&E-stained images for control, BG and BGM groups. * indicates significant differences when compared to the BG group, $*p < 0.05$. Reproduced from ref. 167 with permission from Elsevier [H. Wang, X. Zeng, L. Pang, H. Wang, B. Lin, Z. Deng *et al.*, *Chem. Eng. J.*, 2020, **396**, 125081], copyright 2020.

characteristics. Fluorescence quenching, which arises from fluorescence resonance energy transfer (FRET) between 2D nanomaterials and fluorescent probes or from non-radiative dipole–dipole interactions, is another important property. This characteristic helps reduce fluorescence interference in resonance Raman spectroscopy and is advantageous for 2D nanomaterial-based DNA sensors. Additional benefits of 2D nanomaterials include biocompatibility, high surface area, high electron mobility, and ease of surface modification. 2D nanomaterials are gaining popularity as cancer-targeted imaging possibilities due to these characteristics.[170–173]

Driven by these intrinsic advantages, studies are more focused on engineering 2D nanomaterial-based hybrid systems for multimodal imaging and therapy. For instance, Wang *et al.* developed MoS_2/Bi_2S_3–PEG nanosheets designed for use in multimodal imaging and therapy. The MoS_2 component provides strong performance in photoacoustic imaging and demonstrates high efficiency in converting light to heat for PTT. Meanwhile, Bi_2S_3 offers excellent X-ray attenuation for CT imaging and has a notable ability to absorb photons, which leads to the production of secondary electrons that enhance the effects of radiation therapy. Their findings also showed that these MoS_2/Bi_2S_3–PEG nanosheets are biocompatible, exhibiting no significant toxicity for up to 40 days after intravenous administration, as confirmed by hematological analysis, tissue examination, and tracking of body weight.[78]

In a similar effort to enhance imaging performance through material integration, a nanoparticle system composed of methoxy-polyethylene glycol-*co*-polypyrrole (PEG-*co*-PPyr) and its nanocomposites with MoS_2 were introduced. Experimental results demonstrated that both the mPEG-*co*-PPyr nanoparticles

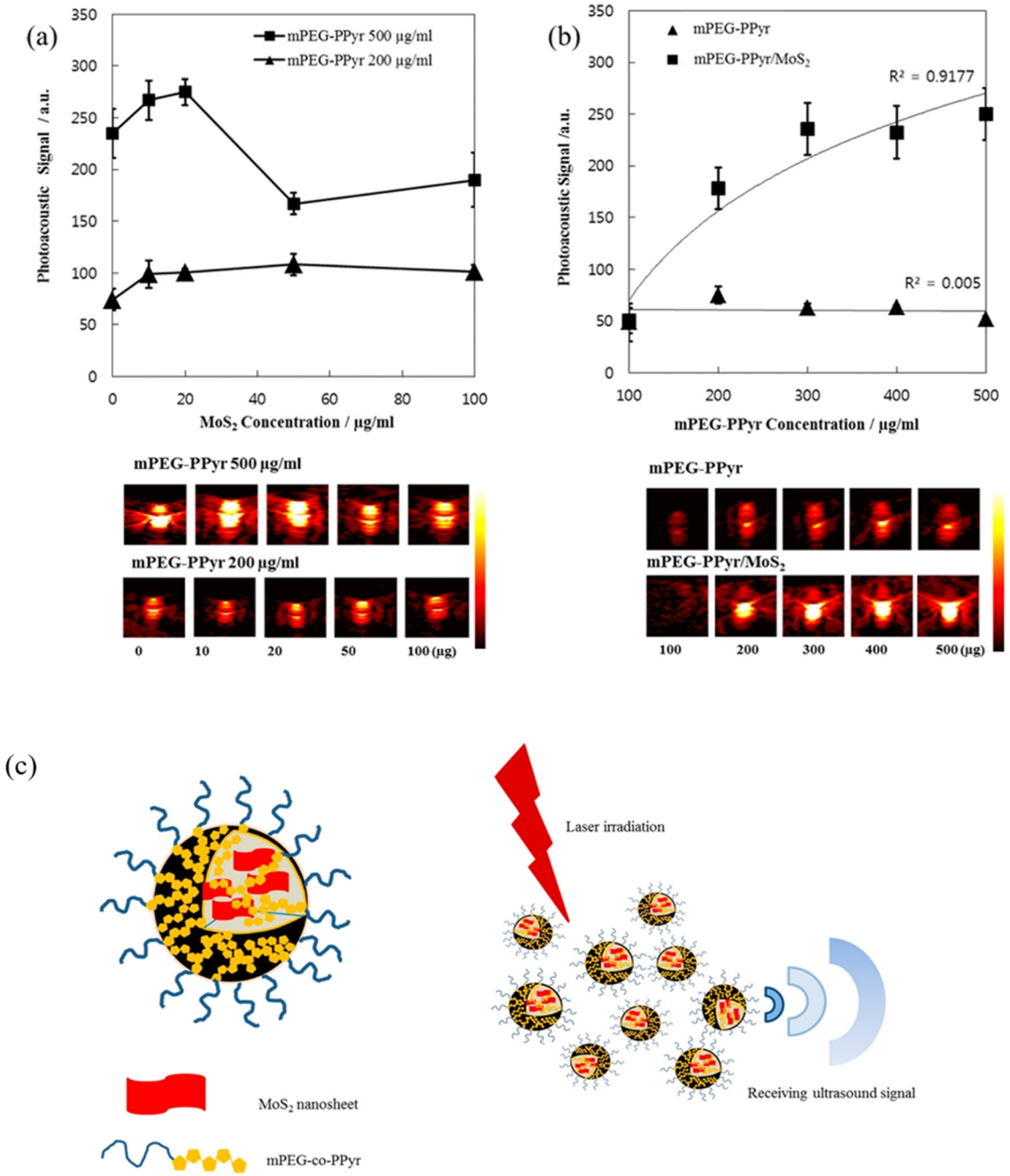

Fig. 10 (a) Photoacoustic responses of mPEG-*co*-PPyr/MoS_2 nanocomposites recorded at different MoS_2 loadings (0–100 μg). (b) PA responses of the nanocomposites measured at a fixed MoS_2 content (20 μg) while varying the amount of mPEG-*co*-PPyr (100–500 μg). (c) Schematic illustration of the mPEG-*co*-PPyr/MoS_2 nanocomposite structure and the mechanism underlying their photoacoustic signal generation. Adapted from ref. 174 with permission from ACS [H. Lee, H. Kim, T. P. Nguyen, J. H. Chang, S. Y. Kim, H. Kim and E. Kang, *ACS Appl. Mater. Interfaces*, 2016, **8**, 29213–29219], copyright 2016.

and the mPEG-*co*-PPyr/MoS_2 nanocomposites generated PA signals. However, the nanocomposites exhibited significantly higher PA signal amplitudes at 700 nm than the stand-alone nanoparticles. In this system, semiconducting polypyrrole served as an electroactive component, while the MoS_2 nanosheets and PEG played critical roles in absorbing near-infrared (NIR) light. The absorbed thermal energy from NIR irradiation was efficiently converted into acoustic waves, enabling enhanced PA imaging. This dual functionality addressed limitations inherent to traditional NIR optical imaging, such as depth-penetration constraints, by combining PA's acoustic detection with optical excitation to improve diagnostic precision (Fig. 10).[174]

4.3. Drug delivery

The rapid advancement of nanotechnology in recent years has highlighted the promise of nanomaterial-based systems for drug

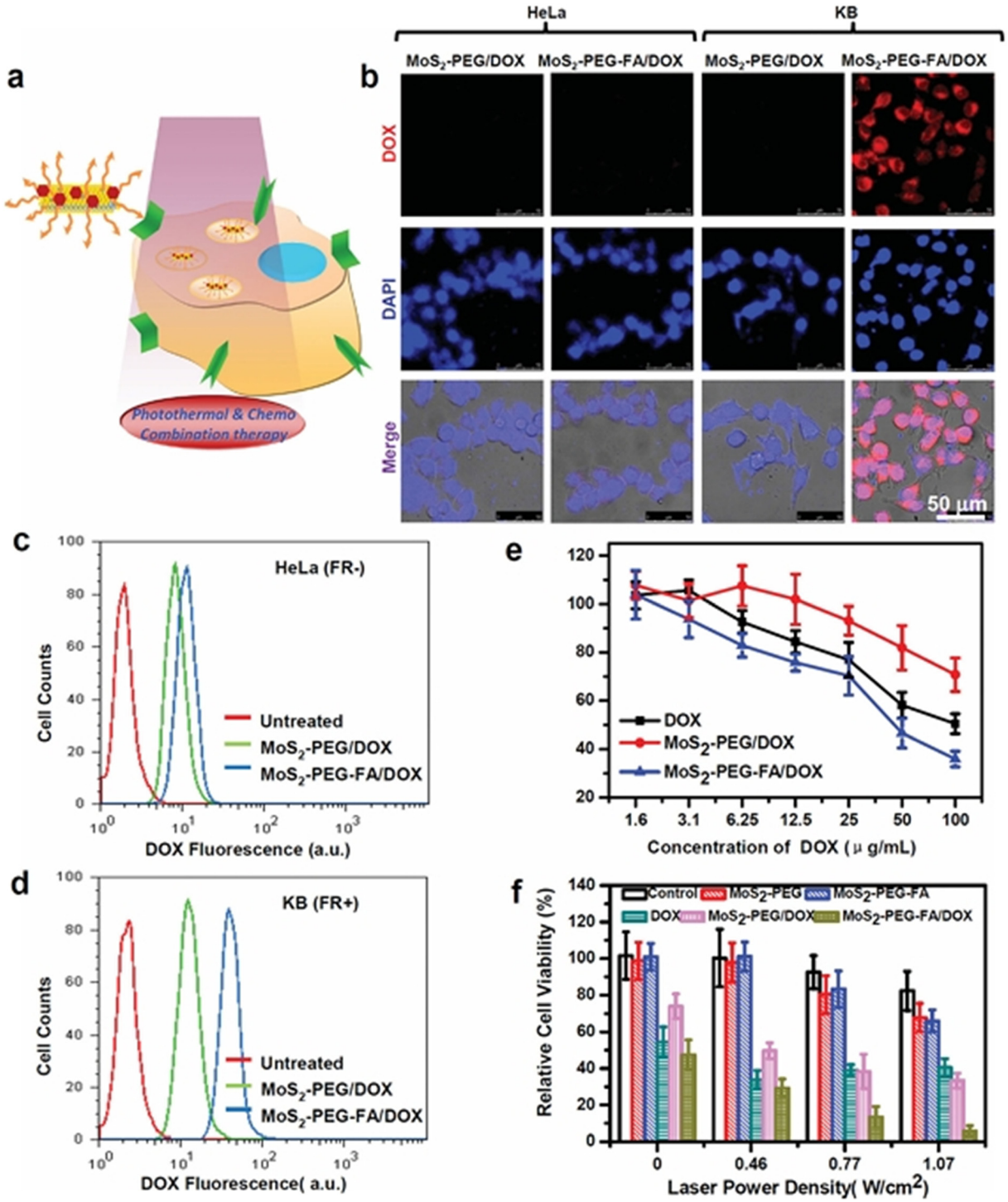

Fig. 11 (a) Schematic representation of the *in vitro* targeted therapy using MoS_2-PEG-FA/DOX. (b) Confocal fluorescence micrographs of HeLa and KB cells following 1 h incubation with MoS_2-PEG/DOX or MoS_2-PEG-FA/DOX. (c and d) Flow cytometric analysis of intracellular DOX fluorescence in HeLa (c) and KB (d) cells after treatment with MoS_2-PEG/DOX or MoS_2-PEG-FA/DOX at the same DOX concentration. (e) Relative viability of KB cells treated with free DOX, MoS_2-PEG/DOX, or MoS_2-PEG-FA/DOX at varying concentrations. After 1 h drug exposure, cells were rinsed with PBS, transferred to fresh medium, and cultured for an additional 24 h before performing the MTT assay. (f) Cell viability of KB cells after various MoS_2-PEG-FA/DOX treatments, with or without 808 nm laser irradiation, followed by 24 h incubation and MTT assessment. Adapted from ref. 12 with permission from Wiley Advanced [T. Liu, C. Wang, X. Gu, H. Gong, L. Cheng, X. Shi, L. Feng, B. Sun and Z. Liu, *Adv. Mater.*, 2014, **26**, 3433], copyright 2014.

delivery. Among these, 2D nanomaterials have emerged as particularly noteworthy owing to their exceptional physical and chemical properties. These materials offer distinctive benefits and considerable potential, especially as platforms for highly

accurate targeted delivery in tumor treatment.[175] Due to their inherent advantages, early efforts have focused on exploiting 2D nanomaterials as high-capacity drug carriers with integrated therapeutic functionalities. In a study demonstrated by Liu *et al.*, PEGylated MoS_2 nanosheets were used as a novel 2D nanocarrier with high drug-loading capacity and good stability for cancer treatment. When loaded with doxorubicin, MoS_2-PEG nanosheets exhibited combined photothermal and chemotherapeutic effects, resulting in significant tumor inhibition in both *in vitro* and *in vivo* studies at lower doses than those of graphene-based agents. Compared to gold nanomaterials, MoS_2-PEG nanosheets have been shown to provide the added benefit of efficient drug delivery, making them more suitable for combination therapy. Although early studies had indicated low toxicity and good biocompatibility, further investigations into long-term safety, metabolism, and biodistribution had been emphasized along with the potential of active targeting strategies to enhance therapeutic efficacy (Fig. 11).[12]

To address the need for enhanced targeting specificity, subsequent studies have incorporated a ligand-mediated approach into 2D nanocarrier design. For instance, a multifunctional MoS_2-based nanocarrier was designed for targeted chemo-photothermal cancer therapy. The nanosheets had been functionalized with folic acid BSA to enable receptor-mediated targeting and further modified with PEG to enhance stability and biocompatibility. The nanoparticle exhibited a uniform particle size of about 133 nm and a high DOX loading capacity of 151.4 mg L^{-1}. Drug release was observed to occur more rapidly under acidic conditions and was further accelerated by NIR irradiation, making it suitable for tumor-specific delivery. Cellular studies confirmed efficient uptake by MDA-MB-231 cancer cells, and the combination of chemotherapy and photothermal therapy led to a significant reduction in cell viability while healthy cells remained largely unaffected, demonstrating the potential of this system for selective cancer treatment.[176]

In parallel with MoS_2-based systems, graphene-derived nanomaterials have also been extensively explored to achieve similar synergistic therapeutic effects. For example, an rGO nanocarrier (MBPEI–PEG–rGO) has been developed for combined chemo-photothermal therapy of hepatocarcinoma. In this system, rGO was employed as the matrix and was functionalized with branched polyethylenimine and polyethylene glycol to improve stability and biocompatibility. The nanocarrier achieved a DOX loading efficiency of 81%. It released more than 50% of DOX under acidic conditions, enabling tumor-targeted delivery and *in vitro* micropinocytosis, resulting in ROS generation, apoptosis, and pronounced cytotoxicity in SMMCS-7721 cells. Moreover, *in vivo* evaluation showed that intratumoral administration of the nanocarrier, followed by local laser irradiation, nearly eliminated hepatocarcinoma.[177]

Extending beyond MoS_2 and graphene-based platforms, BP nanosheets have been proposed as a new material for application in the field of combined cancer therapy owing to their high DOX loading capability compared to other 2D materials. The nanosheets showed much higher DOX loading than other 2D materials, such as graphene and MoS_2. Drug release had been responsive to both acidic conditions and 808 nm laser irradiation, allowing targeted delivery to tumor sites. The BP nanosheets had also functioned as both PTT and PDT agents, and *in vivo* studies had demonstrated effective tumor suppression. Additionally, the system was photostable, biocompatible, and adaptable for delivering other therapeutic molecules, such as DNA, siRNA, or proteins, highlighting its potential as a versatile platform for multifunctional nanomedicine.[8]

4.4. Combination therapies

The latest advancements in designing 2D nanocomposites for synergistic cancer therapy focus on integrating 2D nanomaterials with diverse functional agents, including chemotherapeutic molecules, biomacromolecules, photosensitizers, polymers, and sonosensitizers. This hybridization strategy enhances their multifunctional performance, enabling smart, stimuli-responsive actions triggered by cues such as NIR light, an acidic tumor microenvironment, and redox variations while simultaneously amplifying the combined effects of multiple therapeutic approaches.[178]

In this context, the shift toward combinatorial therapeutic strategies has become particularly significant, as addressing multiple therapeutic targets and using combination therapies have shown great promise in improving cancer treatment efficacy. 2D nanomaterials have a distinct advantage due to their strong NIR light absorption and high photothermal conversion efficiency, making them effective agents for PTT against tumors.[179] Eliminating cancer cells using PTT alone is challenging, particularly for tumors located deep within the body. This difficulty primarily arises from the inherent scattering and absorption of NIR light by biological tissues, which limits light penetration and reduces the treatment's effectiveness.[180] Furthermore, the effectiveness of PTT is limited by cancer cells' ability to survive heat stress, largely because elevated temperatures increase the production of heat shock proteins that help protect cells from thermal damage.[181]

These intrinsic limitations of stand-alone PTT have driven the development of synergistic treatment modalities, wherein hyperthermia is strategically combined with other therapeutic approaches. The observed benefits of hyperthermia include not only killing tumor cells that are resistant to radiotherapy or chemotherapy but also enhancing blood circulation and increasing oxygen concentration within tumors. These effects contribute to significantly boosting the effectiveness of treatments such as chemotherapy, photodynamic therapy, and radiotherapy when used alone.[182] Moreover, the heat generated by PTT can disrupt endosomal membranes, facilitating the escape of genes or drugs from endosomes into the cytoplasm, thereby contributing to highly efficient cancer treatment.[166,183]

Guided by these design principles, recent studies have focused on engineering multifunctional 2D nanoplatforms

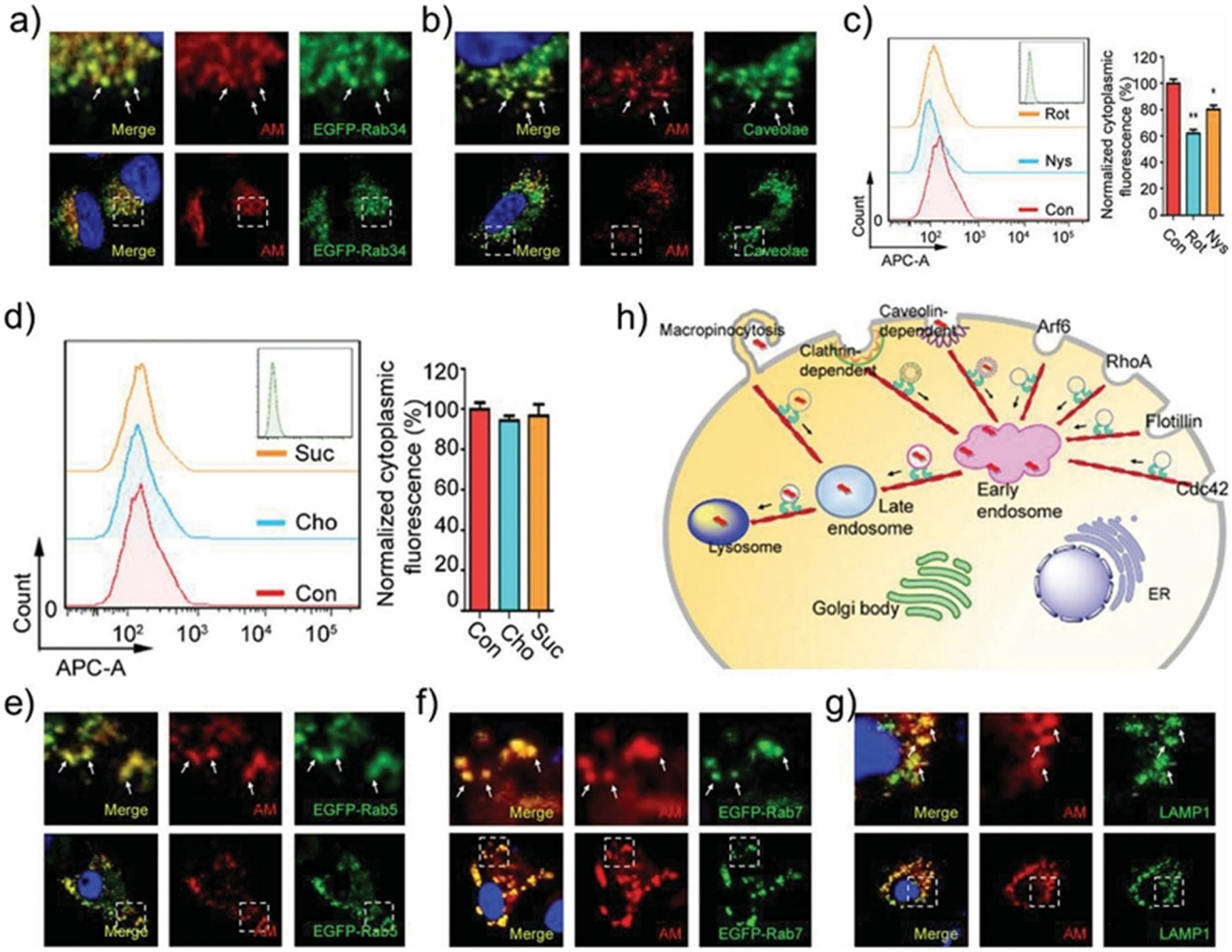

Fig. 12 (a) Macropinocytosis and (b) caveolin-mediated endocytosis pathways. (c) Cytoplasmic fluorescence (FCM) of cells pretreated with micropinocytosis inhibitor (Rot) or caveolin pathway inhibitor (Nys) for 2 h. (d) FCM analysis of cells treated with clathrin-mediated endocytosis inhibitors. Following cellular uptake, AM-PEG nanosheets are trafficked through (e) early endosomes, (f) late endosomes, and (g) lysosomes. (h) Schematic illustration depicting the internalization and intracellular transport of FITC-labeled AM-PEG nanosheets in MCF-7 cells (scale bar: 10 μm). Adapted from ref. 47 with permission from Wiley Advanced [W. Tao *et al.*, *Adv. Mater.*, 2018, **30**, 1802061], copyright 2018.

capable of integrating photothermal effects with controlled drug delivery. 2D antimonene nanosheets (AM NSs) were developed *via* exfoliation of bulk antimony and systematically evaluated for their biodegradability, biocompatibility, and therapeutic performance *in vitro* and *in vivo*. Polyethylene glycol-functionalized AM NSs (AM-PEG) demonstrated strong NIR absorption and a high photothermal conversion efficiency (41.8%), enabling effective photothermal treatment with a high DOX loading capacity of about 150%, attributed to their large surface area. The resulting AM-PEG/DOX nanocomposites exhibited stimulus-responsive (acidic pH, NIR irradiation) drug release and efficient tumor targeting, producing superior anticancer outcomes through combined photothermal and chemotherapeutic effects compared with monotherapy (Fig. 12).[47]

Beyond drug-loaded photothermal systems, efforts have also been directed toward improving targeting efficiency and delivery routes. In this regard, a nanographene oxide–hyaluronic acid (NGO–HA) conjugate was reported that facilitates HA receptor-mediated transdermal uptake into melanoma tissue and exhibits high photothermal conversion efficiency under 808 nm NIR irradiation. Upon topical application and NIR exposure (2 W cm^{-2}, 10 min), the NGO–HA system raised local temperatures by ~40 °C, inducing complete tumor ablation with no recurrence and >96% viability of adjacent fibroblasts. Efficacy was confirmed by elevated caspase-3 activity and TUNEL-positive staining for apoptosis. Additionally, NGO's π– π stacking capacity enables co-loading of chemotherapeutic agents, paving the way for combined transdermal chemo-photothermal therapy (Fig. 13).[184] In parallel, the integration of photothermal and photodynamic functionalities within a single nanoplatform has emerged as a powerful strategy to further enhance therapeutic outcomes. In this context, PEGylated MoS_2 nanosheets that load chlorin e6 at ~30 wt% were used for enhanced photodynamic therapy and, upon 808 nm NIR

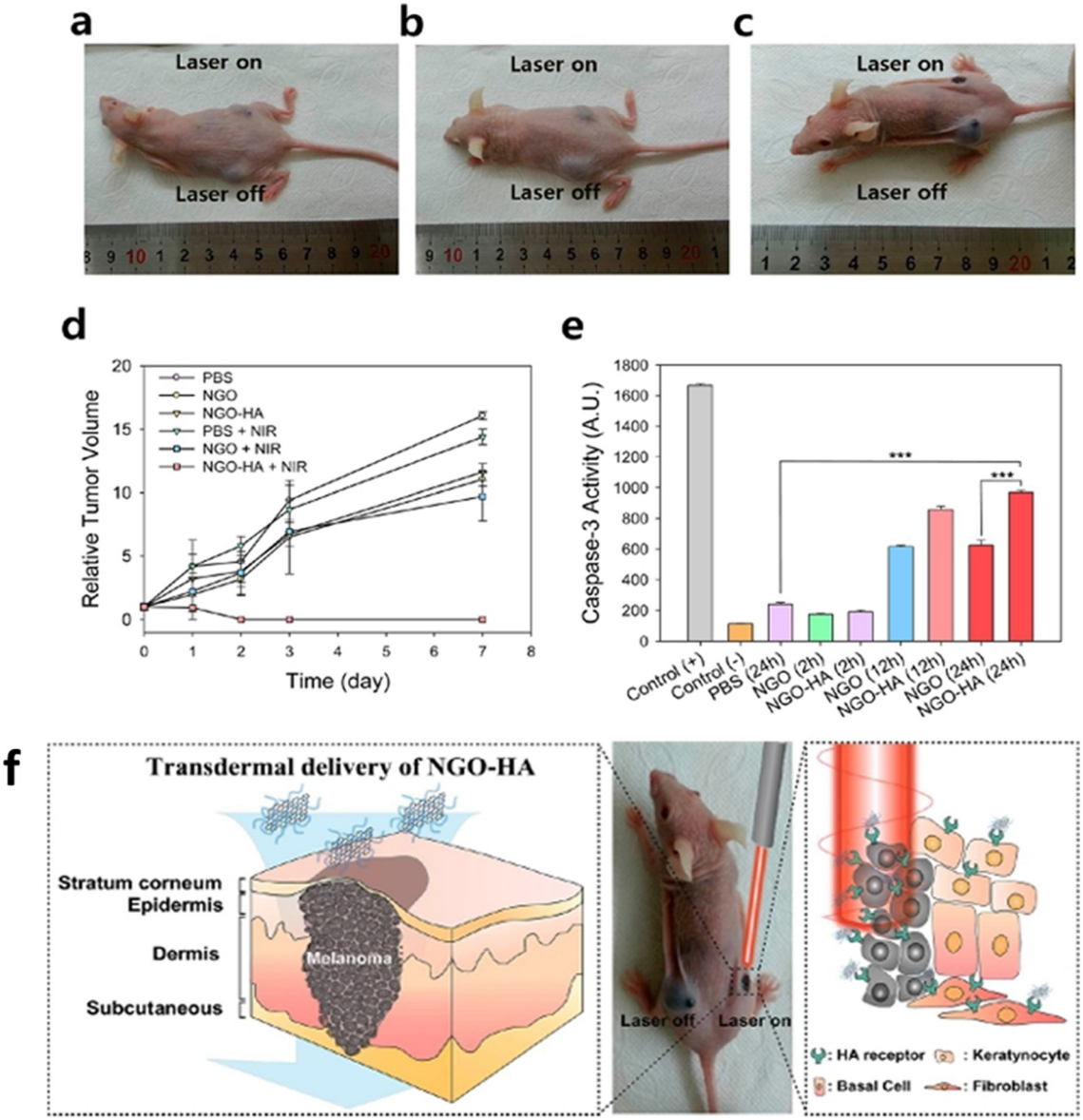

Fig. 13 Photographs illustrating the impact of NIR-triggered PTT on tumor progression in SKH-1 mice bearing B16F1 tumors on both dorsal flanks following topical application of (a) PBS, (b) nanographene oxide (NGO), and (c) NGO–hyaluronic acid. (d) Relative tumor volume monitored over one week. (e) Caspase-3 activity in tumor tissue was measured by ELISA over 24 hours to evaluate heat-induced apoptosis (***$P < 0.0001$). (f) Schematic showing transdermal delivery of NGO–HA conjugates into melanoma cells followed by NIR-induced photothermal ablation therapy. Adapted from ref. 184 with permission from ACS [H. S. Jung, W. H. Kong, D. K. Sung, M.-Y. Lee, S. E. Beack, D. H. Keum *et al.*, *ACS Nano*, 2014, **8**, 260–268], copyright 2014.

irradiation, generate mild hyperthermia (~43 °C) to double cellular drug uptake; combined with 660 nm light, this dual mode treatment achieved synergistic cancer cell killing *in vitro* and markedly greater tumor growth inhibition in 4T1-bearing mice without systemic toxicity.[185]

Extending these findings, further refinement of such dual modal systems has focused on improving photothermal efficiency alongside improving *in vivo* stability and therapeutic precision. In this context, a biocompatible cancer theranostic platform with combined photothermal and photodynamic properties was engineered by decorating ultrathin black phosphorus nanosheets with amine-terminated PEG (BP@PEG) and loading them with the photosensitizer chlorin e6 (Ce6). The resulting BP@PEG/Ce6 nanoparticles maintain colloidal stability in physiological media, achieve approximately 30 wt% Ce6 loading, and convert NIR light to heat with 43.6% efficiency, substantially higher than BP@PEG alone (28.7%). Upon 606 nm irradiation, the particles generate reactive oxygen species from released Ce6, while 808 nm light induces photothermal heating, enabling combined photodynamic and photothermal tumor cell destruction *in vitro*. *In vivo* fluorescence imaging confirmed tumor targeting *via* the enhanced permeability and retention effect, and dual-mode treatment markedly suppressed tumor growth with negligible systemic toxicity.[186]

Furthermore, the focus has shifted toward developing multi-stage, stimuli-responsive systems capable of spatiotemporal control of therapeutic activation. In line with this approach, 2D MoS_2 nanosheets, stabilized with lipoic acid PEG and functionalized with a pH-sensitive charge-reversible peptide, have been engineered to co-deliver the cationic photosensitizer toluidine blue O (TBO). In a physiological environment, TBO is tightly associated with the MoS_2 surface, leading to quenched fluorescence and suppressed reactive oxygen species (ROS) generation, while the anionic peptide coating enhances systemic stability. Upon internalization into tumor cell endo-/lysosomes, the acidic conditions trigger hydrolysis of peptide amide bonds, exposing positive charges that promote cellular uptake, weaken TBO MoS_2 interactions, and initiate TBO release. Subsequent 808 nm irradiation induces mild photothermal heating, which not only damages cancer cells but also accelerates TBO desorption. Finally, 630 nm light irradiation restores TBO fluorescence and ROS generation, enabling potent and selective photodynamic action. This sequential activation strategy results in effective tumor ablation *in vitro* and significant tumor growth inhibition *in vivo* with minimal off-target toxicity.[187]

Thus, a number of 2D nanomaterials, such as graphene derivatives, TMDs, black phosphorus, and MXenes, are considered highly promising for photothermal therapy and many other biomedical applications owing to their unique physical and chemical properties. The thin atomic nature, vast surface area, modifiable electrical property, and high absorbance of UV-vis NIR radiation in these materials make it possible for them to achieve excellent photothermal conversion efficiency and provide the opportunity to modify the surfaces of the materials for precise medical treatments.[57,188] Moreover, the easy-to-implement functionalization strategy enables these platforms to integrate drug delivery, bioimaging, and multimodal therapies into a single system, resulting in improved treatment efficiency.[189] Table 3 summarizes 2D nanomaterials with various surface functionalization along with their photothermal performance and additional biomedical applications, including imaging, drug delivery, and combination therapy.

5. Future perspective and challenges

The development of 2D nanomaterials for cancer theranostics is often told as a story of continuous promise. However, a closer look at recent evidence shows a field struggling between strong preclinical data and ongoing challenges that keep laboratory innovations from reaching clinical use. The idea of multifunctional hybrid platforms, which combine responsive drug delivery, various imaging methods (PAT, CT, MRI), and combined treatments like photothermal, photodynamic, and chemotherapy, is appealing. Yet, it often moves ahead of the thorough understanding required to support these clinical goals.[189,202] Materials such as MXene and BP continue to attract attention for their tunable optical properties and strong NIR absorption, and emerging applications in CRISPR-based gene therapy and immunomodulation of the tumor microenvironment further expand the conceptual horizon.[203] However, interest in these attributes has all too often been disconnected from consideration of their limitations, and the difference between a lab-scale nanosheet and a clinically viable nanomedicine is not only technical but also one of reproducibility, quality control, and manufacturing that the field often acknowledges only in passing. Scalable synthesis through liquid phase exfoliation and chemical vapor deposition is still not well controlled in terms of batch-to-batch variations in defect density, lateral dimensions, and chemistry that regulatory bodies need to see for clinical application.[204,205]

The toxicity issue is also less resolved than many of these reviews acknowledge. Indeed, while materials like MoS_2 and Bi_2S_3 have promising photothermal and imaging properties

Table 3 Different 2D nanoparticles used in PTT and other biomedical applications

Sl. no.	Materials	Surface modification	Laser effect	Applications	Ref.
1	rGO/MTX/SB	$mPEG_{2000}$-NH_2	805 nm, 0.75 W cm^{-2} for 5 min	Photothermal-immunotherapy–chemotherapy	190
2	HPAA/GO-RGD–DOX	RGD–peptide	808 nm, 1.5 W cm^{-2} for 5 min	Combination therapy	191
3	$PdTe_2$	DSPE-PEG	1060 nm, 0.5 W cm^{-2} for 5 min	PTT	192
4	PtAg nanosheets	SH-PEG-FA	[i] 785 nm, 1 W cm^{-2} for 6 min [ii] 1064 nm, 1.4 W cm^{-2} for 6 min	PTT, PA imaging	193
5	CoFeMn dichalcogenide nanosheets	PVP	808 nm, 1 W cm^{-2} for 5–8 min	PTT, PA imaging	194
6	GO/$ZnFe_2O_4$	PEG	980 nm, 0.8 W cm^{-2} for 5 min	PTT, PDT, CT, MRI, PA imaging	195
7	WS_2 nanosheets	PEG	808 nm, 1 W cm^{-2} for 5 min	PT	196
8	DOX–CuS@$CaCO_3$@PL-PEG	PL-PEG	980 nm, 2 W cm^{-2} for 5–10 min	PTT, CDT, chemotherapy	197
9	BcFe@SRF	—	808 nm, 1.5 W cm^{-2} for 5 min	PTT, CDT, chemotherapy	198
10	CuS/TPP@PCM	—	808 nm, 1 W cm^{-2} for 5 min	PTT, drug delivery	199
11	Nisin–Au–rGO	Nisin peptide, gold nanoparticles	800 nm, 0.5 W cm^{-2} for 5 min	PTT, memory device	148
12	Ag/Nd-ZnO/rGO	—	8–32 J cm^{-2}	PTT	200
13	ICG–PDA–rGO	ICG, polydopamine	808 nm, 0.6 W cm^{-2} for 5 min	PTT, PA imaging	201
14	rGO–Ru–PEG	PEG	450 nm, 0.5 W cm^{-2} for 5 min	PTT	149

in animal models, claims of low toxicity are based largely on animal studies of clearance that are not relevant to the human reticuloendothelial system.[205,206] The lack of *in vivo* animal studies to validate the kinetics of biodegradation and organ clearance for non-biodegradable and slowly biodegradable 2D nanosheets is conspicuous. In addition, the long-term toxicity in humans for the entire range of nanomaterials has not been explored. Even though PEGylation has been shown to be effective in improving the stability and preventing non-specific protein adsorption onto nanoparticles, the accelerated blood clearance response that occurs due to the generation of anti-PEG antibodies in the bloodstream has created a problem for the repeated dose regimens that are needed for cancer therapy.[207–209] The field's enduring inclination toward PEGylation is indicative of a propensity to go for tried and true answers rather than questioning whether those solutions are truly appropriate for the particular biological setting of 2D nanosystems.

The tumor biology problem is also underemphasized in optimistic accounts of targeted delivery. The aspirational stories of ligand-functionalized nanosheets that selectively target cancer cells overlook the physical inaccessibility of the tumor microenvironment. The dense stromal microenvironment, comprising collagen and cancer-associated fibroblasts, physically hinders nanoparticle delivery. In addition, heterogeneous vascularization and increased interstitial pressure also impede nanoparticle delivery.[210] This lack of concordance between animal and human tumor architecture is one of the most enduring causes of failed translation in nanomedicine, and yet preclinical studies continue to rely predominantly on subcutaneous xenografts that bear little resemblance to human malignancies.[211] In addition, the regulatory environment is fragmented, and harmonized international standards for the characterization of nanomaterials, including particle size distribution, surface chemistry, quantification of defects, and protein corona dynamics, remain to be developed, making it difficult to achieve cross-laboratory reproducibility and regulatory approval in an unpredictable fashion.[212]

However, the prospect of 2D nanomaterials for cancer theranostics is truly a fascinating area, and the field is poised to take it to the next step. With substantial advancements achieved in the optical performance and therapeutic approaches, scientists have a solid base from which they can tackle the remaining hurdles, such as large-scale production, thorough *in vivo* toxicity studies, biocompatibility, and deep tumor infiltration. Moreover, the power of computational tools and artificial intelligence can speed up the process of finding new materials and optimizing their properties for specific uses, such as targeted drug delivery, efficient photothermal treatment, and enhanced imaging. The next step in the development holds significant promise to strategically expand past simple demonstrations and embrace translational research, fully recognizing the complexities of human tumors, regulatory science, and the possibility of bringing about an actual breakthrough in the use of nanomaterials in cancer management.

6. Conclusion

In conclusion, this review provides a comprehensive exploration of 2D nanomaterials, emphasizing their synthesis strategies, surface functionalization, and multifaceted roles in cancer theranostics. By detailing the structural and functional diversity of materials such as graphene, TMDs, MXenes, and LDHs, it highlights how their unique physicochemical properties enable targeted drug delivery, advanced imaging, and effective photothermal therapy. This discussion integrated recent advancements and experimental findings, offering insights into translational oncology. Substantial progress has been made, overcoming challenges related to large-scale synthesis, reproducibility, and comprehensive toxicity assessments, which are essential for successful clinical translation. Additionally, exploiting computational modeling and artificial intelligence can accelerate the discovery and optimization of 2D nanomaterials, enabling the design of platforms tailored for precise drug delivery, effective photothermal therapy, and advanced imaging. Ultimately, these multidisciplinary efforts have the potential to transform precision oncology, bridging the gap between cutting-edge nanomedicine research and real-world patient care by providing safer, more effective, and patient-specific treatment.

Author contributions

A. M. performed the literature research. J. T. conceptualized the idea. A. M. and J. T. wrote the manuscript.

Conflicts of interest

There are no conflicts of interest.

List of abbreviations

2D	Two-dimensional
LDH	Layered double hydroxide
BP	Black phosphorus
MXenes	Carbonitrides
TMD	Transition metal dichalcogenide
hBN	Hexagonal boron nitride
Pd	Palladium
CVD	Chemical vapor deposition
NIR	Near-infrared
PTT	Photothermal therapy
LPE	Liquid phase exfoliation
GO	Graphene oxide
rGO	Reduced graphene oxide
GDY	Graphydine
NGO	Nano graphene oxide
SiC	Silicon carbide
GNF	Graphene nanoflakes
PSMA	Prostate specific membrane antigen
DFO	Desferroxamine
DOX	Doxorubicin
PLGA	Poly(lactic-*co*-glycolic acid)

rBMSCs	Rat bone mesenchymal stem cells
HF	Hyaluronic acid
TPAOH	Tetrapropylammonium hydroxide
PAI	Photoacoustic imaging
NS	Nanosheet
COOH	Carboxyl
OH	Hydroxyl
–C═O	Carbonyl
–O–	Epoxy
TNF-α	Tumor necrosis factor
PCO	Posterior capsule opacification
LSPR	Localized surface plasmon resonance
T_x	Terminal group
BGM	Borosilicate bioactive glass
$CeMOS_2$	Amphiphilic MOS_2 nanosheet
OI	Optical imaging
MRI	Magnetic resonance imaging
PET	Positron emission tomography
CT	Computed tomography
FRET	Fluorescence resonance energy transfer
PEG-*co*-PPyr	Methoxy-polyethylene glycol-*co*-polypyrrole
MBPEI-PEG-GO	rGO nanocarrier
AM NS	Antimonene nanosheet
AM-PEG	Polyethylene glycol functionalized antimonene nanosheet
NGO–HA	Nano graphene oxide–hyaluronic acid
BP@PEG	Black phosphorus nanosheet with amine-treated PEG
Ce6	Chlorin e6
TBO	Toluidine blue O
ROS	Reactive oxygen species

Data availability

No primary research results have been included, and no new data were generated or analysed as part of this review. Original sources of the data are cited throughout the manuscript.

References

1 H. Niroki and Y. H. Kim, *J. Thorac. Dis.*, 2017, **9**, 448–451.
2 S. Z. Bukhari, K. Zeth, M. Iftikhar, M. Rehman, M. U. Munir, W. S. Khan and A. Ihsan, *Curr. Res. Pharmacol. Drug Discovery*, 2021, **2**, 100067.
3 Y. Song, P. Zhu, Z. Xu and J. Chen, *ACS Appl. Bio Mater.*, 2020, **3**, 5730–5740.
4 L. Cai, P. Zhu, F. Huan, J. Wang, L. Zhou, H. Jiang, M. Ji and J. Chen, *Colloids Surf., B*, 2021, **205**, 111839.
5 W. Pei, Y. Li, Y. Wu, Y. Wu, L. Cai, S. Wang, S. Wang and J. Chen, *Adv. Funct. Mater.*, 2023, **33**, 2308117.
6 W. Pei, L. Cai, X. Gong, L. Zhang, J. Zhang, P. Zhu, H. Jiang, C. Wang, S. Wang and J. Chen, *Mater. Today Bio*, 2022, **15**, 100272.
7 K. Yang, L. Feng, X. Shi and Z. Liu, *Chem. Soc. Rev.*, 2013, **42**, 530.
8 Z. Gu, S. Zhu, L. Yan, F. Zhao and Y. Zhao, *Adv. Mater.*, 2019, **31**, 1800662.
9 H. Lin, S. Gao, C. Dai, Y. Chen and J. Shi, *J. Am. Chem. Soc.*, 2017, **139**, 16235.
10 L. Cheng, J. Liu, X. Gu, H. Gong, X. Shi, T. Liu, C. Wang, X. Wang, G. Liu, H. Xing, W. Bu, B. Sun and Z. Liu, *Adv. Mater.*, 2014, **26**, 1886.
11 T. Liu, S. Shi, C. Liang, S. Shen, L. Cheng, C. Wang, X. Song, S. Goel, T. E. Barnhart, W. Cai and Z. Liu, *ACS Nano*, 2015, **9**, 950.
12 T. Liu, C. Wang, X. Gu, H. Gong, L. Cheng, X. Shi, L. Feng, B. Sun and Z. Liu, *Adv. Mater.*, 2014, **26**, 3433.
13 L. Cheng, C. Yuan, S. Shen, X. Yi, H. Gong, K. Yang and Z. Liu, *ACS Nano*, 2015, **9**, 11090.
14 Y. Chao, G. Wang, C. Liang, X. Yi, X. Zhong, J. Liu, M. Gao, K. Yang, L. Cheng and Z. Liu, *Small*, 2016, **12**, 3967.
15 D. Chimene, D. L. Alge and A. K. Gaharwar, *Adv. Mater.*, 2015, **27**, 7261.
16 Y. Chen, Y. Wu, B. Sun, S. Liu and H. Liu, *Small*, 2017, **13**, 1603446.
17 R. Kurapati, K. Kostarelos, M. Prato and A. Bianco, *Adv. Mater.*, 2016, **28**, 6052.
18 K. Huang, Z. Li, J. Lin, G. Han and P. Huang, *Chem. Soc. Rev.*, 2018, **47**, 5109.
19 X. Qian, Z. Gu and Y. Chen, *Mater. Horiz.*, 2017, **4**, 800.
20 Y. W. Chen, Y. L. Su, S. H. Hu and S. Y. Chen, *Adv. Drug Delivery Rev.*, 2016, **105**, 190.
21 K. Yang, L. Hu, X. Ma, S. Ye, L. Cheng, X. Shi, C. Li, Y. Li and Z. Liu, *Adv. Mater.*, 2012, **24**, 1868.
22 C. Wang, J. Li, C. Amatore, Y. Chen, H. Jiang and X.-M. Wang, *Angew. Chem., Int. Ed.*, 2011, **50**, 11644.
23 B. Sels, D. De Vos, M. Buntinx, F. Pierard, A. Kirsch-De Mesmaeker and P. Jacobs, *Nature*, 1999, **400**, 855.
24 F. Song and X. Hu, *Nat. Commun.*, 2014, **5**, 4477.
25 K. Fan, H. Chen, Y. Ji, H. Huang, P. M. Claesson, Q. Daniel, B. Philippe, H. Rensmo, F. Li, Y. Luo and L. Sun, *Nat. Commun.*, 2016, **7**, 11981.
26 L. Li, Y. Yu, G. J. Ye, Q. Ge, X. Ou, H. Wu, D. Feng, X. H. Chen and Y. Zhang, *Nat. Nanotechnol.*, 2014, **9**, 372.
27 X. Wang, A. M. Jones, K. L. Seyler, V. Tran, Y. Jia, H. Zhao, H. Wang, L. Yang, X. Xu and F. Xia, *Nat. Nanotechnol.*, 2015, **10**, 517.
28 D. Hanlon, *et al.*, *Nat. Commun.*, 2015, **6**, 8563.
29 J. Shao, *et al.*, *Nat. Commun.*, 2016, **7**, 12967.
30 Z. Sun, *et al.*, *Angew. Chem., Int. Ed.*, 2015, **54**, 11526.
31 B. Anasori, M. R. Lukatskaya and Y. Gogotsi, *Nat. Rev. Mater.*, 2017, **2**, 16098.
32 F. Shahzad, *et al.*, *Science*, 2016, **353**, 1137.
33 H. H. Hwu and J. G. Chen, *Chem. Rev.*, 2005, **105**, 185.
34 T. Rodenas, *et al.*, *Nat. Mater.*, 2015, **14**, 48.
35 M. Zhao, *et al.*, *Chem. Soc. Rev.*, 2018, **47**, 6267.
36 L. Ma, C. Abney and W. Lin, *Chem. Soc. Rev.*, 2009, **38**, 1248.
37 S. Zhao, *et al.*, *Nat. Energy*, 2016, **1**, 16184.
38 Y. Ding, *et al.*, *J. Am. Chem. Soc.*, 2017, **139**, 9136.
39 S. Manzeli, *et al.*, *Nat. Rev. Mater.*, 2017, **2**, 17033.
40 C. Tan and H. Zhang, *Chem. Soc. Rev.*, 2015, **44**, 2713.

41 J. N. Coleman, *et al.*, *Science*, 2011, **331**, 568.
42 Q. H. Wang, *et al.*, *Nat. Nanotechnol.*, 2012, **7**, 699.
43 M. Chhowalla, *et al.*, *Nat. Chem.*, 2013, **5**, 263.
44 K. Watanabe, T. Taniguchi and H. Kanda, *Nat. Mater.*, 2004, **3**, 404.
45 X. Ji, *et al.*, *Adv. Mater.*, 2018, **30**, 1803031.
46 W. Tao, *et al.*, *Angew. Chem., Int. Ed.*, 2017, **56**, 11896.
47 W. Tao, *et al.*, *Adv. Mater.*, 2018, **30**, 1802061.
48 X. Huang, *et al.*, *Nat. Nanotechnol.*, 2011, **6**, 28.
49 V. Nicolosi, *et al.*, *Science*, 2013, **340**, 1226419.
50 K. S. Novoselov, *et al.*, *Science*, 2004, **306**, 666.
51 Z. Chen, *et al.*, *Nat. Mater.*, 2011, **10**, 424.
52 A. N. Obraztsov, *Nat. Nanotechnol.*, 2009, **4**, 212.
53 Z. Cai, B. Liu, X. Zou and H. M. Cheng, *Chem. Rev.*, 2018, **118**, 6091.
54 L. Cheng, X. Wang, F. Gong, T. Liu and Z. Liu, *Adv. Mater.*, 2020, **32**, 1902333.
55 J. Shen, Y. Zhu, X. Yang and C. Li, *Chem. Soc. Rev.*, 2015, **44**, 2157–2178.
56 X. Qi, H. Zhang, J. Wu, Z. Zhang and X. Liu, *Adv. Drug Delivery Rev.*, 2021, **173**, 179–201.
57 S. Liu, X. Pan and H. Liu, *Angew. Chem.*, 2020, **59**, 5890–5900.
58 P. T. Yin, S. Shah, M. Chhowalla and K. B. Lee, *Chem. Rev.*, 2015, **115**, 2483.
59 B. Yang, Y. Chen and J. Shi, *Chem*, 2018, **4**, 1284.
60 C. Murugan, V. Sharma, R. K. Murugan, G. Malaimegu and A. Sundaramurthy, *J. Controlled Release*, 2019, **299**, 1.
61 L. Wang, Q. Xiong, F. Xiao and H. Duan, *Biosens. Bioelectron.*, 2017, **89**, 136.
62 I. S. Raja, M. S. Kang, K. S. Kim, Y. J. Jung and D.-W. Han, *Cancers*, 2020, **12**, 1657.
63 T. Rimza, S. Singh and P. Kumar, in *Biosensor-Based Advanced Cancer Diagnostics*, Academic Press, 2022, pp. 321–331.
64 J.-J. Hu, Y.-J. Cheng and X.-Z. Zhang, *Nanoscale*, 2018, **10**, 22657.
65 Y. Chen, Z. Fan and Z. Zhang, *Chem. Rev.*, 2018, **118**, 6409.
66 C. Tan, X. Cao and X.-J. Wu, *et al.*, *Chem. Rev.*, 2017, **117**, 6225.
67 H. Zhang, *ACS Nano*, 2015, **9**, 9451.
68 N. Abid, A. M. Khan and S. Shujait, *et al.*, *Adv. Colloid Interface Sci.*, 2022, **300**, 102597.
69 M. Adel, M. A. Ahmed and A. A. Mohamed, *J. Phys. Chem. Solids*, 2021, **149**, 109760.
70 X. Guo, Z. Fan, Y. Wang and Z. Jin, *Surf. Interfaces*, 2021, **24**, 101105.
71 C. Sun, L. Wen and J. Zeng, *et al.*, *Biomaterials*, 2016, **91**, 81.
72 S. Nazir, M. U. A. Khan and W. S. Al-Arjan, *et al.*, *Arabian J. Chem.*, 2021, **14**, 103120.
73 H. Lin, Y. Wang, S. Gao, Y. Chen and J. Shi, *Adv. Mater.*, 2018, **30**, 1703284.
74 S. Karimi, H. Rasuli and R. Mohammadi, *Int. J. Biol. Macromol.*, 2023, **234**, 123538.
75 M. J. Shabbir, R. Aqeel and M. Hassan, *et al.*, *Synth. Met.*, 2024, **309**, 117775.
76 H. Wang, J. Zhou and Y. Fu, *et al.*, *Adv. Healthcare Mater.*, 2021, **10**, 2100536.
77 B. Li, G. Fu and C. Liu, *et al.*, *J. Colloid Interface Sci.*, 2024, **665**, 389.
78 S. Wang, X. Li and Y. Chen, *et al.*, *Adv. Mater.*, 2015, **27**, 2775.
79 D. de Melo-Diogo, C. Pais-Silva, D. R. Dias, A. F. Moreira and I. J. Correia, *Adv. Healthcare Mater.*, 2017, **6**, 1700073.
80 R. Faria, T. Albuquerque and A. R. Neves, *et al.*, *J. Mol. Liq.*, 2020, **316**, 113873.
81 E. P. Randviir, D. A. C. Brownson and C. E. Banks, *Mater. Today*, 2014, **17**, 426.
82 C. R. Minitha, M. Lalitha, Y. L. Jeyachandran, L. Senthilkumar and R. T. Rajendrakumar, *Mater. Chem. Phys.*, 2017, **194**, 243.
83 M. Yi and Z. Shen, *J. Mater. Chem. A*, 2015, **3**, 11700.
84 H. Ji, H. Sun and X. Qu, *Adv. Drug Delivery Rev.*, 2016, **105**, 176.
85 V. Palmieri, M. D. Spirito and M. Papi, *Nanomedicine*, 2020, **15**, 1411.
86 D. Wu, J. Li and S. Xu, *et al.*, *J. Am. Chem. Soc.*, 2020, **142**, 19602.
87 J. H. Jung, D. S. Cheon, F. Liu, K. B. Lee and T. S. Seo, *Angew. Chem., Int. Ed.*, 2010, **49**, 5708.
88 B. G. Choi, H. Park and T. J. Park, *et al.*, *ACS Nano*, 2010, **4**, 2910.
89 Q. He, H. G. Sudibya and Z. Yin, *et al.*, *ACS Nano*, 2010, **4**, 3201.
90 H. N. Bhatt, J. Pena-Zacarias and E. Beaven, *et al.*, *ACS Appl. Bio Mater.*, 2023, **6**, 365.
91 N. K. Mehra, A. K. Jain and M. Nahar, *Drug Discovery Today*, 2018, **23**, 1016.
92 B. Jiang, B. Zhou, Z. Lin, H. Liang and X. Shen, *Chem. – Eur. J.*, 2019, **25**, 3993.
93 S. Hatamie, M. M. Ahadian and M. A. Ghiass, *et al.*, *Colloids Surf., B*, 2016, **146**, 271.
94 J. Lamb, E. Fischer, M. Rosillo-Lopez, C. G. Salzmann and J. P. Holland, *Chem. Sci.*, 2019, **10**, 8880.
95 M. S. Baktash, A. Zarrabi, E. Avazverdi and N. M. Reis, *J. Mol. Liq.*, 2021, **322**, 114515.
96 X. Chang, Y. Zhang and P. Xu, *et al.*, *Carbon*, 2018, **138**, 397.
97 S. J. Cheng, H. Y. Chiu and P. V. Kumar, *et al.*, *Biomater. Sci.*, 2018, **6**, 813.
98 M. Chhowalla, Z. Liu and H. Zhang, *Chem. Soc. Rev.*, 2015, **44**, 2584–2586.
99 Q. Song, X. Pan and H. Wang, *et al.*, *Sci. Rep.*, 2016, **6**, 29254.
100 G. A. Ermolaev, *et al.*, *Nat. Commun.*, 2021, **12**, 854.
101 H. Zhao, Q. Guo, F. Xia and H. Wang, *Nanophotonics*, 2015, **4**, 128–142.
102 H. Li, J. Wu, Z. Yin and H. Zhang, *Acc. Chem. Res.*, 2014, **47**, 1067–1075.
103 H. Wang, X. Zeng and L. Pang, *et al.*, *Chem. Eng. J.*, 2020, 396.
104 S. Hajian, *et al.*, *IEEE Sensors*, 2018, pp. 1–4.
105 X. Jiang, A. V. Kuklin and A. Baev, *et al.*, *Phys. Rep.*, 2020, **848**, 1–58.
106 T. L. Tan, H. M. Jin, M. B. Sullivan, B. Anasori and Y. Gogotsi, *ACS Nano*, 2017, **11**, 4407–4418.

107 A. C. Rajan, A. Mishra, S. Satsangi, R. Vaish, H. Mizuseki, K.-R. Lee and A. K. Singh, *Chem. Mater.*, 2018, **30**, 4031–4038.
108 T. Hu, M. Hu, B. Gao, W. Li and X. Wang, *J. Phys. Chem. C*, 2018, **122**, 18501–18509.
109 H. Lin, Y. Chen and J. Shi, *Adv. Sci.*, 2018, **5**, 1800518.
110 A. K. Gaharwar, *et al.*, *Adv. Mater.*, 2019, **31**, 1900332.
111 F. Bergaya and G. Lagaly, *Handbook of Clay Science*, Newnes, 2013.
112 J. Madejová, J. Kečkéš, H. Pálková and P. Komadel, *Clay Miner.*, 2002, **37**, 377–388.
113 X. Ji, *et al.*, *Nat. Commun.*, 2021, **12**, 1124.
114 X. Ji, *et al.*, *Adv. Sci.*, 2019, **6**, 1901211.
115 C. Tan, *et al.*, *Chem. Rev.*, 2017, **117**, 6225–6331.
116 Y. Kuthati, R. K. Kankala and C.-H. Lee, *Appl. Clay Sci.*, 2015, **112**, 100–116.
117 J. He, M. Wei, B. Li, Y. Kang, D. G. Evans and X. Duan, in *Layered Double Hydroxides*, Springer, 2006, pp. 89–119.
118 Z. Ye, Y. Bao, Z. Chen, H. Ye, Z. Feng and Y. Li, *et al.*, *Coord. Chem. Rev.*, 2024, **504**, 215654.
119 J. Liu, X. Zheng and L. Yan, *ACS Nano*, 2019, **13**, 9740–9752.
120 H. Lin, Y. Wang, S. Gao, Y. Chen and J. Shi, *Adv. Mater.*, 2017, **30**, 1703284.
121 C. Dai, Y. Chen, X. Jing, L. Xiang, D. Yang and H. Lin, *et al.*, *ACS Nano*, 2023, **17**, 9593–9608.
122 Z. Chen, X. Chen, G. Liu, K. Han, J. Chen and J. Wang, *Front. Bioeng. Biotechnol.*, 2022, **10**, 886109.
123 Z. Jiang, M. Zhang, P. Li, Y. Wang and Q. Fu, *Theranostics*, 2023, **13**, 483.
124 W. Zhou, Y. Jia, Y. Liu, Y. Chen and P. Zhao, *Pharmaceutics*, 2022, **14**, 2346.
125 S. Wang, Y. Chen, X. Li, W. Gao, L. Zhang and J. Liu, *et al.*, *Adv. Mater.*, 2015, **27**, 7117–7122.
126 S. Malekmohammadi, H. Hadadzadeh, H. Farrokhpour and Z. Amirghofran, *Soft Matter*, 2018, **14**, 2400–2410.
127 J. Wang, H. Zhang, X. Xiao, D. Liang, X. Liang, L. Mi, J. Wang and J. Liu, *Acta Biomater.*, 2020, **107**, 260–271.
128 S.-L. Chen, C.-Y. Chen and J. C.-H. Hsieh, *et al.*, *Nanomaterials*, 2019, **9**, 1725.
129 S. Li, Y. Qing, Y. Lou, R. Li, H. Wang and X. Wang, *et al.*, *Int. J. Biol. Macromol.*, 2023, **239**, 124209.
130 S. Xu, Y. Zhong, C. Nie, Y. Pan, M. Adeli and R. Haag, *Macromol. Biosci.*, 2021, **21**, e2100233.
131 X. M. Han, K. W. Zheng and R. L. Wang, *et al.*, *Am. J. Transl. Res.*, 2020, **12**, 1515–1534.
132 Y. Liu, D. Zhu, X. Zhu, G. Cai, J. Wu, M. Chen, P. Du, Y. Chen, W. Liu and S. Yang, *Chem. Sci.*, 2020, **11**, 11435–11442.
133 Z. Chen, W. Wang and Y. Li, *et al.*, *Mol. Pharmaceutics*, 2021, **18**, 386–402.
134 Z. Lv and L. Yang, *Mol. Med. Rep.*, 2013, **8**, 345–349.
135 L. Cao, *et al.*, *Acc. Chem. Res.*, 2013, **46**, 171–180.
136 J.-L. Li, *et al.*, *Biomaterials*, 2013, **34**, 9519–9534.
137 J. R. Melamed, R. S. Edelstein and E. S. Day, *ACS Nano*, 2015, **9**, 6–11.
138 M. Pérez-Hernández, P. del Pino, S. G. Mitchell, M. Moros, G. Stepien, B. Pelaz, W. J. Parak, E. M. Gálvez, J. Pardo and J. M. de la Fuente, *ACS Nano*, 2015, **9**, 52–61.
139 B. Shah, D. Khunt, H. Bhatt, M. Misra and H. Padh, *J. Drug Delivery Sci. Technol.*, 2016, **33**, 37–50.
140 S. V. K. Rompicharla, H. Bhatt, A. Shah, N. Komanduri, D. Vijayasarathy, B. Ghosh and S. Biswas, *Chem. Phys. Lipids*, 2017, **208**, 10–18.
141 S. M. Sharker, *Int. J. Nanomed.*, 2019, **14**, 9983–9993.
142 N. C. D. Nath, T. Debnath, M. Nurunnabi and E.-K. Kim, in *Biomedical Applications of Graphene and 2D Nanomaterials*, ed. M. Nurunnabi and J. R. McCarthy, Elsevier, 2019, pp. 165–186.
143 P. Kalluru, R. Vankayala, C.-S. Chiang and K. C. Hwang, *Biomaterials*, 2016, **95**, 1–10.
144 W. Gao, in *Graphene Oxide: Reduction Recipes, Spectroscopy, and Applications*, Springer International Publishing, Cham, 2015, pp. 61–95.
145 S. Goenka, V. Sant and S. Sant, *J. Controlled Release*, 2014, **173**, 75–88.
146 R. Muñoz, D. P. Singh, R. Kumar and A. Matsuda, in *Nanostructured Polymer Composites for Biomedical Applications*, ed. S. K. Swain and M. Jawaid, Elsevier, 2019, pp. 447–488.
147 M. J. Feito, M. Vila, M. C. Matesanz, J. Linares, G. Gonçalves, P. A. A. P. Marques, M. Vallet-Regí, J. M. Rojo and M. T. Portolés, *J. Colloid Interface Sci.*, 2014, **432**, 221–228.
148 S. V. Otari, M. Kumar, M. Z. Anwar, N. D. Thorat, S. K. S. Patel, D. Lee, J. H. Lee, J.-K. Lee, Y. C. Kang and L. Zhang, *Sci. Rep.*, 2017, **7**, 10980.
149 D.-Y. Zhang, Y. Zheng, C.-P. Tan, J.-H. Sun, W. Zhang, L.-N. Ji and Z.-W. Mao, *ACS Appl. Mater. Interfaces*, 2017, **9**, 6761–6771.
150 Y. He, W. Cao, C. Cong, X. Zhang, L. Luo, L. Li, H. Cui and D. Gao, *ACS Sustainable Chem. Eng.*, 2019, **7**, 3584–3592.
151 L. Zhu, M. Gao, C. K. N. Peh and G. W. Ho, *Mater. Horiz.*, 2018, **5**, 323–343.
152 D. Xu, Z. Li, L. Li and J. Wang, *Adv. Funct. Mater.*, 2020, **30**, 2000712.
153 S. B. Lee, J. M. Park, R. Park, H. E. Choi, S. W. Hong and K. S. Kim, *J. Controlled Release*, 2025, **382**, 113729.
154 S. Shurbaji, N. P. A. Manaph, S. M. Ltaief, A. R. Al-Shammari, A. Elzatahry and H. C. Yalcin, *Front. Nanotechnol.*, 2021, **3**, 689718.
155 H. S. Hao, H. C. Han, Z. Y. Yang, M. Chen, Y. Y. Jiang and F. Wang, *et al.*, *Nano-Micro Lett.*, 2022, **14**, 178.
156 D. B. Wang, Y. X. Fang, W. Yu, L. L. Wang and H. Q. Xie, *et al.*, *Sol. Energy Mater. Sol. Cells*, 2021, **220**, 110850.
157 X. Q. Fan, L. Liu, X. Jin, W. T. Wang and S. F. Zhang, *et al.*, *J. Mater. Chem. A*, 2019, **7**, 14319–14327.
158 Z. Li, Y. Chen, Y. Sun and X. Zhang, *ACS Nano*, 2021, **15**, 5189–5200.
159 T. He, C. Jiang, J. He, Y. Zhang and G. He, *et al.*, *Adv. Mater.*, 2021, **33**, 2008540.
160 J. M. Luther, P. K. Jain, T. Ewers and A. P. Alivisatos, *Nat. Mater.*, 2011, **10**, 361–366.
161 A. R. Mallah, M. N. M. Zubir, O. A. Alawi, K. M. S. Newaz and A. B. M. Badry, *Sol. Energy Mater. Sol. Cells*, 2019, **201**, 110084.

162 V. Mauchamp, M. Bugnet, E. P. Bellido, G. A. Botton and P. Moreau, *et al.*, *Phys. Rev. B: Condens. Matter Mater. Phys.*, 2014, **89**, 235428.
163 A. D. Dillon, M. J. Ghidiu, A. L. Krick, J. Griggs and S. J. May, *et al.*, *Adv. Funct. Mater.*, 2016, **26**, 4162–4168.
164 A. V. Mohammadi, J. Rosen and Y. Gogotsi, *Science*, 2021, **372**, abf1581.
165 X. He, Y. Lv, Y. Lin, H. Yu, Y. Zhang, Y. Tong and C. Zhang, *Adv. Mater.*, 2024, **36**, 2400366.
166 Y. Liu, P. Bhattarai, Z. Dai and X. Chen, *Chem. Soc. Rev.*, 2019, **48**, 2053–2108.
167 H. Wang, X. Zeng, L. Pang, H. Wang, B. Lin and Z. Deng, *et al.*, *Chem. Eng. J.*, 2020, **396**, 125081.
168 S. S. Chou, B. Kaehr, J. Kim, B. M. Foley, M. De, P. E. Hopkins, J. Huang, C. J. Brinker and V. P. Dravid, *Angew. Chem., Int. Ed.*, 2013, **52**, 4160–4164.
169 X. Li, X. N. Zhang, D. X. Li and J. Chang, *Cancer Biol. Med.*, 2016, **13**, 339–346.
170 C. Xin, J. X. Zheng, Y. T. Su, S. K. Li, B. K. Zhang, Y. C. Feng and F. Pan, *J. Phys. Chem. C*, 2016, **120**, 22663–22671.
171 H. F. Dong, W. C. Gao, F. Yan, H. X. Ji and H. X. Ju, *Anal. Chem.*, 2010, **82**, 5511–5517.
172 L. M. Xie, X. Ling, Y. Fang, J. Zhang and Z. F. Liu, *J. Am. Chem. Soc.*, 2009, **131**, 9890–9891.
173 M. Orecchioni, R. Cabizza, A. Bianco and L. G. Delogu, *Theranostics*, 2015, **5**, 710–723.
174 H. Lee, H. Kim, T. P. Nguyen, J. H. Chang, S. Y. Kim, H. Kim and E. Kang, *ACS Appl. Mater. Interfaces*, 2016, **8**, 29213–29219.
175 L. Ding, M. Liang, C. Li, X. Ji, J. Zhang and W. Xie, *et al.*, *Small Methods*, 2022, **6**, 2200853.
176 X. Zhang, J. Wu, G. R. Williams, S. Niu, Q. Qian and L.-M. Zhu, *Colloids Surf., B*, 2019, **173**, 101–108.
177 C. Tong, X. Zhang, J. Fan, B. Li, B. Liu, M. Daniyal and W. Wang, *Sci. Bull.*, 2018, **63**, 935–943.
178 W. Chen, J. Ouyang, H. Liu, M. Chen, K. Zeng and J. Sheng, *et al.*, *Adv. Mater.*, 2017, **29**, 1603864.
179 Y. Chen, C. Tan, H. Zhang and L. Wang, *Chem. Soc. Rev.*, 2015, **44**, 2681–2701.
180 X. Wang, F. Li, X. Yan, Y. Ma, Z.-H. Miao, L. Dou, H. Chen, Y. Lu and Z. Zha, *ACS Appl. Mater. Interfaces*, 2017, **9**, 41782–41793.
181 S. Wang, Y. Tian, W. Tian, J. Sun, S. Zhao and Y. Liu, *et al.*, *ACS Nano*, 2016, **10**, 8578–8590.
182 G. Song, L. Cheng, Y. Chao, K. Yang and Z. Liu, *Adv. Mater.*, 2017, **29**, 1700996.
183 W. Yang, W. Guo, W. Le, G. Lv, F. Zhang and L. Shi, *et al.*, *ACS Nano*, 2016, **10**, 10245–10257.
184 H. S. Jung, W. H. Kong, D. K. Sung, M.-Y. Lee, S. E. Beack and D. H. Keum, *et al.*, *ACS Nano*, 2014, **8**, 260–268.
185 T. Liu, C. Wang, W. Cui, H. Gong, C. Liang, X. Shi, Z. Li, B. Sun and Z. Liu, *Nanoscale*, 2014, **6**, 11219–11225.
186 X. Yang, D. Wang, Y. Shi, J. Zou, Q. Zhao and Q. Zhang, *et al.*, *ACS Appl. Mater. Interfaces*, 2018, **10**, 12431–12440.
187 M.-Y. Peng, D.-W. Zheng, S.-B. Wang, S.-X. Cheng and X.-Z. Zhang, *ACS Appl. Mater. Interfaces*, 2017, **9**, 13965–13975.
188 H. Ma and M. Xue, *J. Mater. Chem. A*, 2021, **9**, 17569–17591.
189 Y. Tan, H. M. Khan, B. A. Sheikh, H. Sun, H. Zhang, J. Chen, D. Huang, X. Chen, C. Zhou and J. Sun, *Front. Bioeng. Biotechnol.*, 2023, **11**, 1141631.
190 X. Zhu, J. Lei, C. Jiang, Z. Fang, W. Zhang and Z. Yang, *et al.*, *Mater. Today Bio*, 2025, **32**, 101668.
191 J. Luo, M. Fan, L. Xiong, Q. Hao, M. Jiang, Q. He and C. Su, *ACS Appl. Mater. Interfaces*, 2021, **13**, 27963–27971.
192 Y. Zhang, Q. Shen, Q. Li, P. He, J. Li and F. Huang, *et al.*, *Adv. Sci.*, 2021, **8**, 2100386.
193 Y. Zhu, Y. Wang, G. R. Williams, L. Fu, J. Wu and H. Wang, *et al.*, *Adv. Sci.*, 2020, **7**, 2000272.
194 H. Bi, F. He, Y. Dai, J. Xu, Y. Dong and D. Yang, *et al.*, *Inorg. Chem.*, 2018, **57**, 9988–9998.
195 R. Bahadur, B. Singh, D. Rai and R. Srivastava, *ACS Appl. Bio Mater.*, 2023, **6**, 4740–4748.
196 X. Yang, H. Zhang, Z. Wu, Q. Chen, W. Zheng and Q. Shen, *et al.*, *J. Controlled Release*, 2024, **376**, 646–658.
197 B. Liu, C. Li, G. Chen, B. Liu, X. Deng and Y. Wei, *et al.*, *Adv. Sci.*, 2017, **4**, 1600540.
198 R. Shao, X. Qiao, L. Cao, J. Man, L. Guo and L. Li, *et al.*, *Discover Nano*, 2023, **18**, 122.
199 B. Liu, H. Jiang, J. Dong, W. Zhang, G. Dang and M. Yang, *et al.*, *Colloids Surf., B*, 2020, **185**, 110590.
200 S. Jafarirad, E. Hammami Torghabe, S. H. Rasta and R. Salehi, *Artif. Cells, Nanomed., Biotechnol.*, 2018, **46**, 800–816.
201 Y. Hu, D. Sun, J. Ding, L. Chen and X. Chen, *J. Mater. Chem. B*, 2016, **4**, 929–937.
202 M. R. Osanloo, *et al.*, *Graphene 2D Mater.*, 2024, **9**, 159–185.
203 A. Bigham, M. Serrano-Ruiz, M. Caporali, I. Fasolino, M. Peruzzini and L. Ambrosio, *et al.*, *Chem. Soc. Rev.*, 2025, **54**, 827–897.
204 R. Sekar and S. Raju, in *Targeted Cancer Therapy in Biomedical Engineering*, 2023, pp. 563–595.
205 X. Yu, C. Xu, J. Sun, H. Xu, H. Huang and Z. Gan, *et al.*, *J. Nanobiotechnol.*, 2024, **22**, 515.
206 H. Li, R. Fan, B. Zou, J. Yan, Q. Shi and G. Guo, *J. Nanobiotechnol.*, 2023, **21**, 73.
207 E. A. C. Ruiz, K. E. Swindle-Reilly and A. N. F. Versypt, *J. Controlled Release*, 2023, **363**, 464–483.
208 Y.-C. Lin, B.-M. Chen, T. T. M. Tran, T.-C. Chang, T. S. Al-Qaisi and S. R. Roffler, *J. Controlled Release*, 2023, **354**, 354–367.
209 Y. Tian, Z. Gao, N. Wang, M. Hu, Y. Ju and Q. Li, *et al.*, *J. Am. Chem. Soc.*, 2022, **144**, 18419–18428.
210 J. Kim, H. Cho, D.-K. Lim, M. K. Joo and K. Kim, *Int. J. Mol. Sci.*, 2023, **24**, 10082.
211 L. N. M. Nguyen, W. Ngo, Z. P. Lin, S. Sindhwani, P. MacMillan and S. M. Mladjenovic, *et al.*, *Nat. Rev. Bioeng.*, 2024, **2**, 201–213.
212 I.-A. Vagena, C. Malapani, M.-A. Gatou, N. Lagopati and E. A. Pavlatou, *Appl. Sci.*, 2025, **15**, 3189.